A Distribution System Harmonic Compensation Approach Using DG-grid Interfacing Converters at Low Switching Frequency

by

Xiaohan Wen

A thesis submitted in partial fulfillment of the requirements for the degree of

Master of Science

in

Energy Systems

Department of Electrical and Computer Engineering
University of Alberta

Abstract

In recent years, embedding ancillary functions of distributed generation (DG) have drawn great attention due to the increasing penetration of renewable energy based DG such as photovoltaic, wind turbines and fuel cells. Among these ancillary functions, harmonics compensation is becoming more interesting and important with the growth of nonlinear loads in today's power distribution system. When controlled properly, the DG-grid interfacing converters can provide effective harmonic compensation for the distribution power system.

However, the conventional harmonic control methods used for active power filters (APFs) may not be suitable for DG units, where the flow of real and reactive power limits the switching frequency to be lower than APFs, especially when the capacity of DG is large. At this low switching frequency, harmonic compensation performance or even the system stability may be affected. In this thesis, a harmonic compensation approach suitable for DG-grid interfacing converters at low switching frequency is proposed.

Acknowledgement

First of all, I would like to gratefully and sincerely thank my supervisor Prof. Yunwei (Ryan) Li for his continuous support and guidance with great patience and enthusiasm during my whole graduate study and research in University of Alberta. Without his patient guidance, this research would not have been possible.

I would also like to thank all the colleagues in Dr. Li's group especially Ye (Eric) Zhang and Yujuan Lian and Farzam Nejabatkhah for their constructive advices and discussions on my research.

Last but not least, I would like to express my gratitude to my parents for encouraging and supporting me throughout my life.

Contents

List of Figures

List of Tables

List of Abbreviations

DG	Distributed generation
RES	Renewable energy sources
DC	Direct Current
AC	Alternating Current
VSI	Voltage source inverter
APF	Active power filter
IRP	Instantaneous reactive power
CCM	Current control method
VCM	Voltage control method
PCC	Point of common coupling
THD	Total harmonic distortion
MPPT	Power point tracking
PR	Proportional and resonant
PWM	Pulse width modulation
ZOH	Zero-order hold
SDFT	Sliding discrete Fourier transform
PV	Photovoltaic

Chapter 1

Introduction

Due to the growing concerns regarding costs and pollution caused by fossil fuel energy, more and more distributed generation (DG) units based on renewable energy sources (RES) such as photovoltaic, wind turbines and fuel cells are being connected to the grid as means to provide power [1]-[4]. Since most DG units have DC or uncontrolled AC output which is not ready for grid integration, a power electronics converter is used to interconnect DG units to the utility grid [5], [6].

The DG interfacing converters can significantly impact the power flow and voltage conditions of the DG system and may introduce harmonics. If controlled and designed properly, the DG interfacing converters are able to provide many different ancillary services to improve power quality and system efficiency [7]-[17]. Among these ancillary functions, harmonics compensation is predicted to play an interesting and important role as the number of nonlinear loads is growing rapidly in today's power distribution system [11]-[16]. In this thesis, a harmonic compensation approach using DG-grid interfacing converter at low switching frequency is proposed, which reduces switching losses.

In Chapter 1, the ancillary services using DG interfacing converter are introduced in brief at first. Then the traditional harmonic distortion mitigation methods for DG systems including the conventional harmonic compensation method using DG interfacing converter are also reviewed. And finally the research objectives and the thesis layout are provided.

1.1 Ancillary Services through DG-grid Interfacing Converter

Sufficient apparent power rating is available for the most DG units based on RES for much of the time due to the nature of intermittent renewable source. Therefore, besides the primary purpose of DG units to generate real power, many ancillary services can be provided through proper control strategies of DG interfacing converter. These ancillary services include reactive power compensation [7], imbalance voltage compensation [8]-[10], load current harmonics compensation [11]-[16], flicker mitigation [17], generation reserve [18], etc.

So far, the most popularly adopted ancillary function of DG systems is probably the reactive power compensation for grid voltage support. This voltage support can be from a high power wind farm, or as small as a single phase PV system. In general, most DG systems use voltage source inverters (VSIs) as their interfacing converters for grid integration. A typical VSI with output LCL filter is shown in Fig. 1.1. And the control scheme of DG to realize the reactive power support can be expressed in Fig. 1.2. By injecting or absorbing reactive power properly, the DG interfacing converter can achieve the corresponding voltage support functions.

Note that for most of the above mentioned ancillary functions, the DG is mainly controlled for real and reactive power regulation, where a high control bandwidth is not necessary for DG and these functions can be relatively easily implemented in the existing DG systems. However, harmonic compensation requires a current control loop that can handle high frequency harmonics, and therefore present a challenge in the DG control scheme, especially when the DG's interfacing converter has low switching frequency to reduce switching losses. Realizing harmonic compensation ancillary function of DG at a low switching frequency is indeed the focus of this thesis.

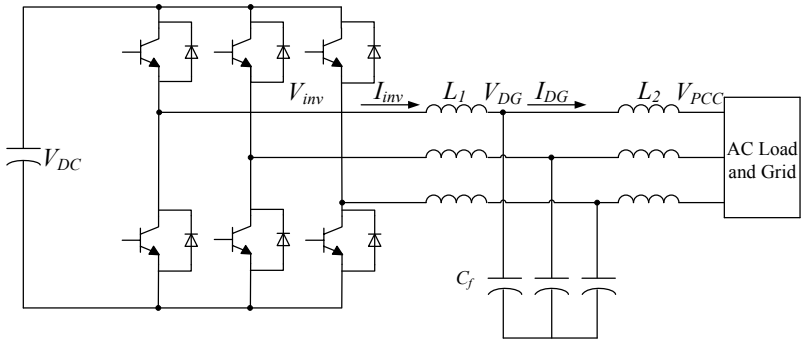

Fig. 1.1 Three-Phase VSI with output LCL filter

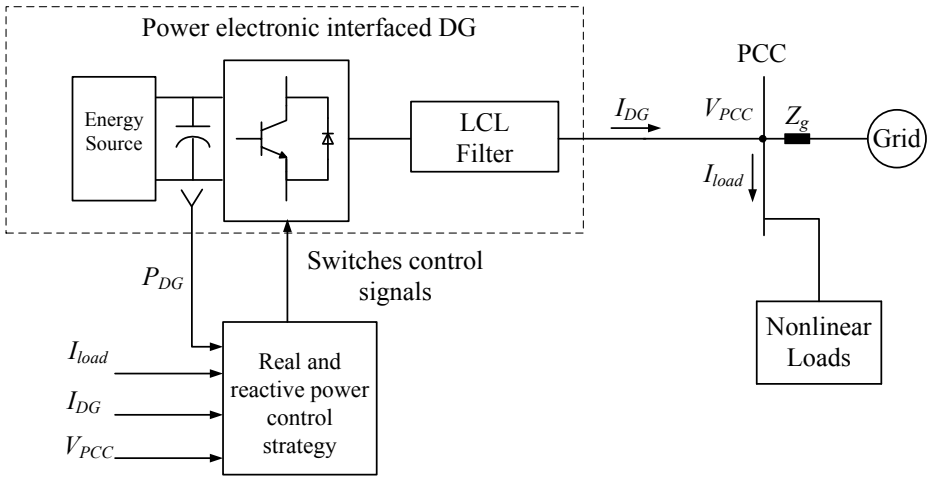

Fig. 1.2 Control scheme of DG to realize the reactive power support

1.2 Traditional Harmonic Distortion Mitigation Methods for DG Systems

In a power distribution system, harmonic currents generated by nonlinear loads produce voltage harmonics, and the harmonics can be amplified by the phenomena of harmonic propagation. Although the individual equipment satisfies standards such as IEC 61000, the aggregate nonlinear loads in a power distribution system may still draw sufficient current harmonics which can lead to excitation of harmonic resonance, especially when line impedance is high such as

in low-voltage distribution and parallel capacitors are added to compensate reactive power.

To compensate these harmonics, passive harmonic filters which consist of capacitors, inductors and resistors are widely used because of their low cost and high reliability. However, passive filters are not very flexible in applications and may introduce additional resonances when they interact with other components in the DG system. To overcome the drawback of conventional passive filters, two kinds of power electronics conditioners are adopted to compensate harmonics. One is active power filter (APF) [19]-[22], and the other one is the DG-grid interfacing converter with the ancillary function of harmonic compensation [11]-[16]. In this section, the conventional harmonic compensation methods using APFs and DG-grid interfacing converters are introduced respectively.

1.2.1 Harmonic mitigation using APFs

Typically, APFs can be divided into shunt active power filters and series active power filters. Fig. 1.3 (a) shows a system configuration of a shunt active power filter, in which the APF is connected in parallel with the nonlinear load and the nonlinear load is a diode rectifier with a capacitive dc load. Shunt APFs are the most widely used and fundamental configuration among all kinds of pure and hybrid APFs. In Fig. 1.3 (a), the harmonic current i_{Lh} of the detected load current i_L at certain frequencies is extracted. Then the active power filter is controlled to

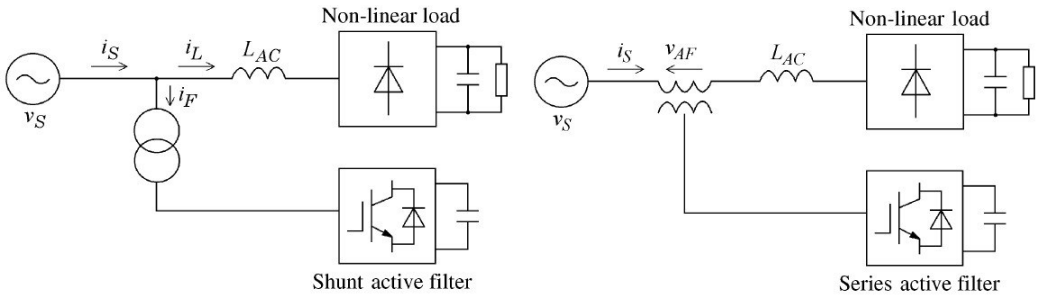

Fig. 1.3 (a) Shunt active power filter. (b) Series active power filter.

produces the compensating current i_F which is equal to $-i_{Lh}$ to achieve harmonic mitigation. In Fig. 1.3 (b), the active filter is connected in series with the mains through a matching transformer. Similarly, based on the extracted harmonic current i_{Sh} in the detected supply current i_S, the active power filter generates the compensating voltage v_{AF} across the primary of transformer. The compensating voltage v_{AF} can be expressed as $-Gi_{Sh}$. When the feedback gain G is set suitably, the supply harmonic currents can be reduced significantly. The converters which are applied for three-phase APFs can be a voltage source converter with a dc capacitor, or a current source converter with a dc inductor. The comparison of voltage source and current source shunt APFs are implemented in details from different points of view in [23]. In addition, many different kinds of hybrid active power filters which can be regarded as the combinations of voltage source converters and passive components are proposed to achieve the purposes such as harmonic isolation between the supply and the nonlinear load [24] and the voltage stress reduction across the switches in active filter [25].

The traditional APFs have been located close to the major nonlinear loads to mitigate harmonics [19] [20]. There are two problems with them. To begin with, this approach is suitable for consumer-funded APFs to compensate harmonics of specific high power nonlinear loads, but it does not suit a collection of many small nonlinear loads that emit correlated low order harmonics [16]. Secondly, most APFs can compensate local nonlinear harmonic currents but cannot compensate the existing network distortion, and the APFs based on instantaneous reactive power (IRP) theory induce additional harmonics if the network voltage is unbalanced [26] [27]. As mentioned previously, sufficient apparent power rating is available for the DG units based on RES due to the nature of intermittent renewable sources. And DG units are located across the network so that they may close to the load centres which require services. Furthermore, considering the fact that installing many APFs at intervals along feeders is not attractive to utility-network operators from economic point of view, harmonic compensation using the DG interfacing converter is a promising topic. The conventional harmonic

compensation methods using the DG interfacing converter are introduced as follows.

1.2.2 Conventional harmonic compensation method based on CCM

As mentioned above, voltage source inverters are widely adopted as DG interfacing converters. And the control schemes of voltage source inverters can be classified into two main types: current control method (CCM) and voltage control method (VCM). The conventional CCM based harmonic compensation method using DG interfacing converter is reviewed at first, in which the DG unit is controlled as a resistive-APF (R-APF) [11]-[12], [21].

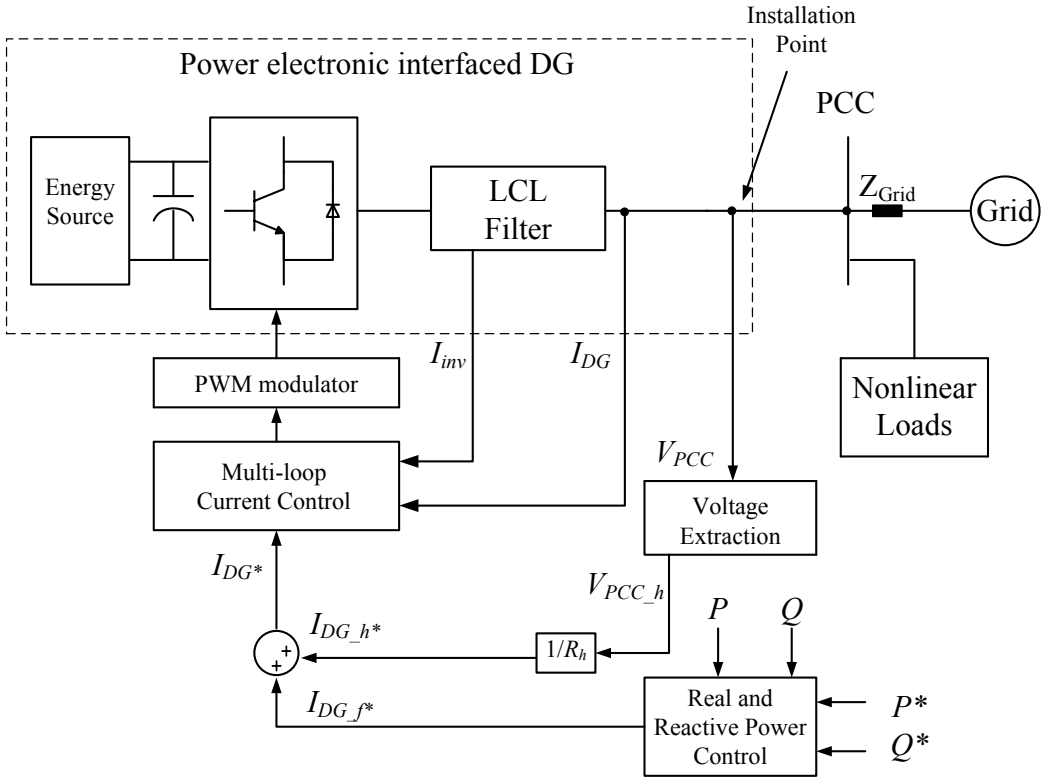

Fig. 1.4 Conventional CCM based harmonic control strategy

Fig. 1.4 shows the block diagram of the conventional harmonic compensation method based on CCM. For the harmonics component, the harmonic currents of the nonlinear loads are absorbed by the DG unit since the DG unit is controlled as a small virtual resistance R_h at harmonic frequencies, leaving an improved grid current and PCC (point of common coupling) voltage with lower THD (total harmonic distortion). The DG current reference consists of a fundamental component for power flow control and a harmonic component to realize the harmonics compensation. The PCC harmonic voltage V_{PCC_h} is extracted to produce the DG harmonic current reference $I_{DG\_h}^{*}$ ($I_{DG\_h}^{*}=V_{PCC\_h}/R_h$). It is worthwhile to note that the voltage of PCC may be difficult to measure remotely under practical situation, therefore the voltage of installation point which is close to PCC voltage can be measured as PCC voltage. In the control scheme shown in Fig. 1.4, the fundamental current reference $I_{DG\_f}^{*}$ is obtained from DG's real and reactive power control in the stationary α-β frame. In the real and reactive power loop, the real power reference can be derived from a maximum power point tracking (MPPT) device or a command value produced by a microgrid energy management center, while the reactive power reference can be obtained from voltage support requirements or load power factor compensation algorithms.

To achieve proper fundamental and harmonics tracking performance, the parallel PR controllers [28] [29] are used as the outer DG current loop controller as illustrated in Fig. 1.5.The PR controller transfer function can be expressed as:

$$K_p + \sum_h \frac{2K_{ih}\omega_{ch}\,\mathrm{s}}{\mathrm{s}^2 + 2\omega_{ch}\mathrm{s} + \omega_h^2} \tag{1.1}$$

where ω_h is the fundamental and harmonic frequencies, ω_{ch} is the cut-off bandwidth, K_{ih} is the integral gain for different frequencies and K_p is the proportional gain for all frequencies. In addition, the inverter output current I_{inv} tracking loop with a proportional controller K_C is added as the inner loop control to improve the dynamic response and stability of the control scheme as shown in Fig. 1.5. In addition, to extract the harmonics selectively, resonant filters [15] or the sliding discrete Fourier transform (SDFT) [30] can be used. And the value of

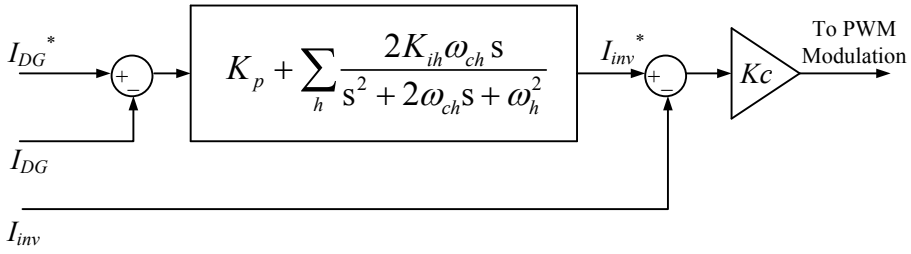

Fig. 1.5 Multi-loop current tracking diagram

R_h can be determined according to an adaptive control algorithm such as proposed in [31] [32] in order to avoid the conflicts between the primary function of power rejection and the harmonic compensation.

The conventional CCM based harmonic compensation method at a relatively high switching frequency is implemented in the simulation. The parameters of the single DG-grid system are listed in Table 1.1, and a diode rectifier is used as the nonlinear load at PCC. The power rating of DG unit is 10 kW and the switching frequency is 12 kHz. The harmonic compensation performance is shown in Fig. 1.6. It is can be seen that the THD of PCC voltage is reduced from 13.77% without compensation to 3.14% with the conventional CCM based harmonic compensation method. As a result, the conventional harmonic compensation method based on CCM is effective when the switching frequency is relatively high (12 kHz).

Table 1.1 Parameters of the single DG-grid system (f_{sw}=12 kHz)

Grid voltage	380V, 60Hz (3 phase)
Grid impedance	R_g=1Ω, L_g=2 mH
LCL filter	L_1=0.2 mH, L_2=0.2 mH, C=10 uF,
DC link voltage	600V
Switching Frequency	12 kHz
Power reference	P*=10 kW, Q*=0 Var

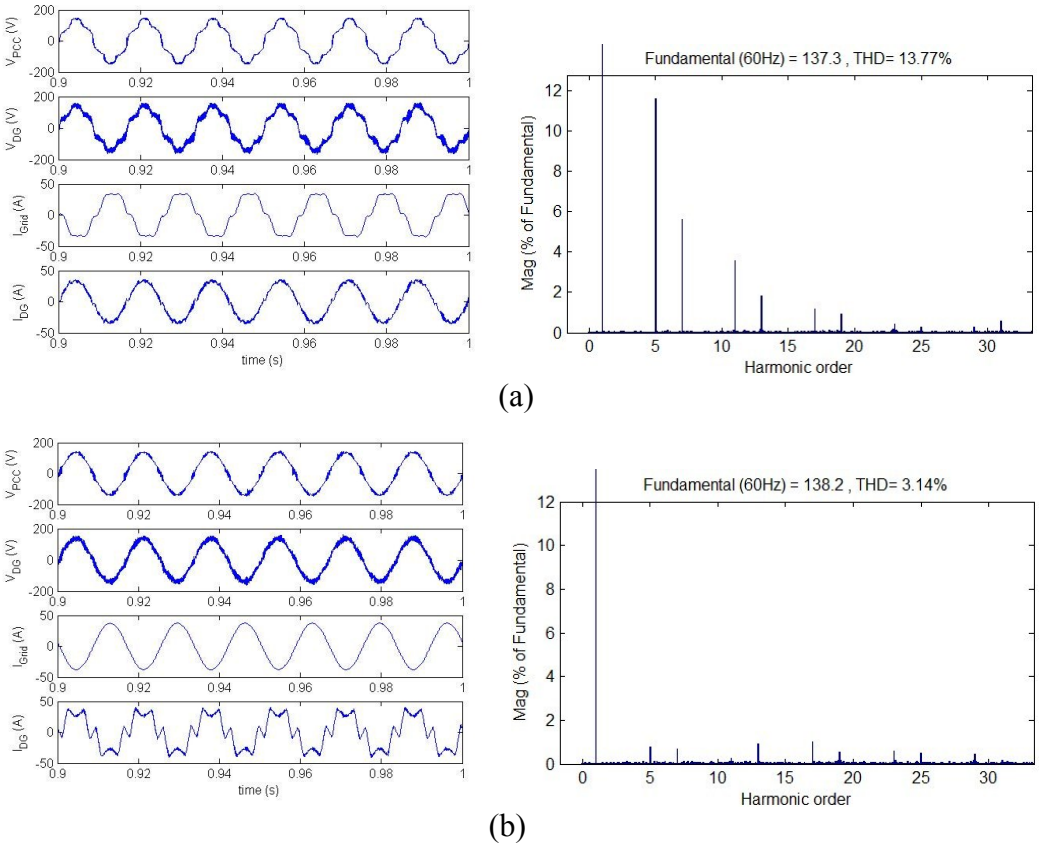

Fig. 1.6 Harmonic compensation performance of PCC voltage (P=10 kW, f_{sw}=12 kHz). (a) Without compensation. (b) Conventional CCM based harmonic compensation method.

1.2.3 Conventional harmonic compensation method based on VCM

The block diagram of the conventional harmonic compensation method based on VCM is shown in Fig. 1.7. For the harmonic component, the PCC harmonic voltage V_{PCC_h} is extracted to produce the DG harmonic voltage reference $V_{DG\_h}^*$ and the DG unit is controlled as a small virtual impedance [11]. The multi-loop voltage control in the VCM based compensation is similar to the multi-loop current control. As shown in Fig. 1.8, the parallel PR controllers for the fundamental and harmonic components are used as the outer voltage loop controller to control the DG output voltage. And the inner proportional current

control loop uses the inverter output current as feedback to improve the dynamic response and stability of the control scheme.

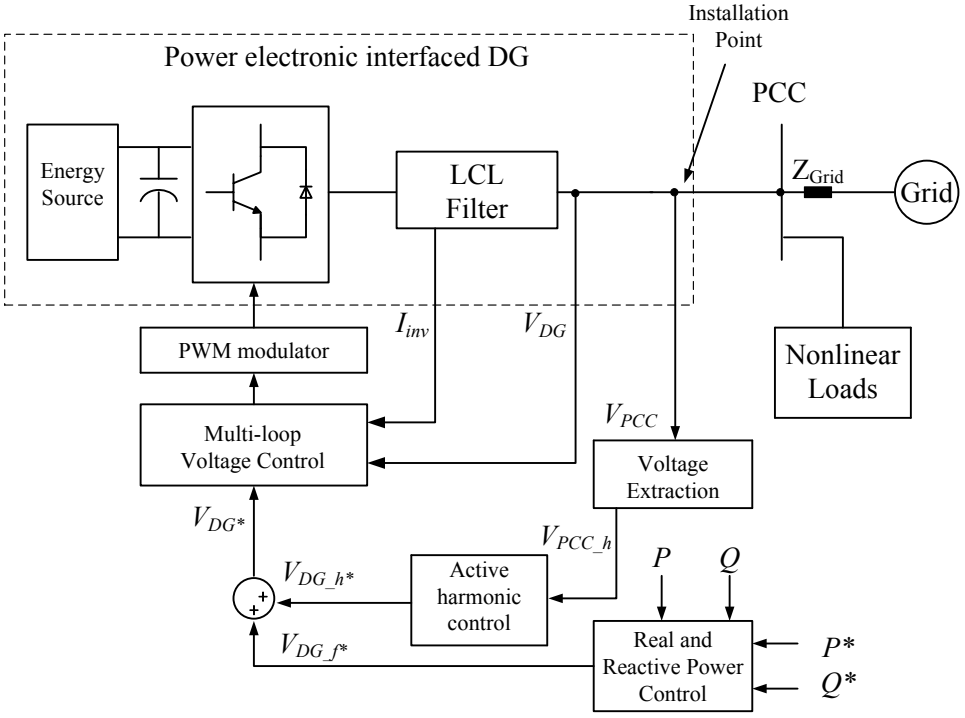

Fig. 1.7 Conventional VCM based harmonic control strategy

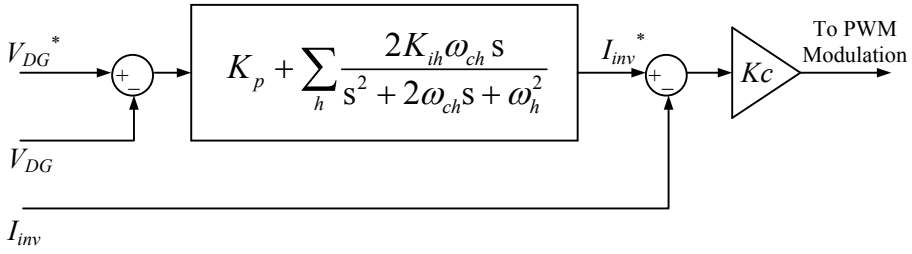

Fig. 1.8 Multi-loop voltage tracking diagram

Traditionally, the current control method is mostly employed for the DG interfacing converter to mitigate harmonics. However, the current control scheme cannot provide direct voltage and frequency support for the loads when the DG system operates in intentional islanding mode. The voltage control method can produce seamless control transition since the VCM based control scheme can be used for both grid-connected mode and intentional islanding mode [11], [33]. And

the VCM based *V-f* droop control (reactive power-magnitude droop and real power-frequency droop) can be applied to regulate the sharing of load demands. Moreover, when the CCM based method is applied only to control power injection without harmonic compensation, all the harmonic currents are pushed to the grid side resulting in the polluted PCC voltage because of the harmonic voltage drop on the grid impedance. But without harmonic compensation, the DG unit based on VCM control scheme can share the harmonic currents of the nonlinear load with the grid.

1.3 DG at Relatively Low Switching Frequencies

The power rating ranges of principal types of DG systems are shown in Table 1.2 [18]. Since the main role of the DG interfacing converter is to control the active and reactive power rejection, its power rating is usually far greater than traditional APFs whose main function is to eliminate harmonics. And the switching frequency of the DG interfacing converter is also limited and lower that of APF converter to reduce switching losses (e.g. a few kHz for DG units compared to more than 10 kHz for APFs).

Table 1.2 Principal types of distributed generation systems

Type	Power range
Wind energy systems	100 kW – 2 MW
Photovoltaic	5 kW – 100 kW
Fuel cells	100 kW – 2 MW
Microturbines	25 kW – 1 MW

To illustrate the challenge of harmonics compensation for DG units with relatively lower switching frequency and higher power rating than APFs, the design criteria of LCL filter also need to be considered as follows [34]-[36].

- The value of capacitor is limited by the decrease of the power factor at rated power. To reduce the absorbed reactive power, the value of capacitor C should be less than or equal to ($\lambda P/2\pi fE^2$), where P is the active power

absorbed by the converter in rated conditions, E is the line to line rms voltage, f is the grid frequency and λ is the ratio of the reactive power absorbed by the capacitor.

- The ac voltage drop on LCL-filter inductance during operation should be less than 10% of the normal grid voltage. Moreover, the ripple attenuation should be considered to limit the current ripple generated by the voltage source converter.
- To avoid resonance problems in the lower and upper harmonic parts, the range of the resonant frequency should be between ten times the grid frequency and one-half of the switching frequency.

Therefore, the relatively lower switching frequency and higher power rating will result in larger filter size, lower filter cutoff frequency and longer delays in the control loop, which subsequently reduce the voltage or current control loop bandwidth. This low control bandwidth will affect the harmonics compensation, especially when the compensation scheme is realized by modifying the current or voltage reference to compensate high order harmonics as in the traditional CCM and VCM based harmonic compensation methods.

Table 1.3 Parameters of the single DG-grid system (f_{sw}=2 kHz)

Grid voltage	380V, 60Hz (3 phase)
Grid impedance	R_g=1Ω, L_g=2 mH
LCL filter	L_1=2 mH, L_2=2 mH, C=40 uF,
DC link voltage	800V
Switching Frequency	2 kHz
Power reference	P*=20 kW, Q*=0 Var

To evaluate the stability of the conventional methods at low switching frequencies, the typical CCM based harmonic compensation method is implemented at a relatively low switching frequency (2 kHz) in the simulation. The parameters of the single DG-grid system are listed in Table 1.3, in which the parameters of LCL filter are modified according to the changes of switching

frequency and power rating. According to the CCM based control scheme shown in Fig. 1.9, the pole positions of the closed loop transfer function I_{DG}/I_{DG}^{*} are calculated and shown in Fig. 1.10, in which the conventional method is applied to control fundamental current and compensate 11th harmonic with the proper control parameters for fundamental and different 11th harmonic integral gain K_{i11} (K_{i11} changes from 1 to 20) of the PR controller. As illustrated in Fig. 1.10, with the increase of 11th harmonic integral gain, the poles of the conventional compensation method move to the right side of the imaginary axis, and the boundary limit of K_{i11} is 5. Therefore, the system described in Table 1.3 is not stable for most 11th harmonic integral gains when using the conventional harmonic compensation method. Fig 1.11 shows the Bode magnitude plot of the open loop transfer function when the 11th harmonic integral gain is set as its maximum value (K_{i11}=5) that makes the system stable. It can be seen that the magnitude at 11th harmonic (660 Hz) is only 2.1 dB, which means an unsatisfactory compensation or even making harmonic performance worse. In conclusion, the conventional method is not suitable to compensate high frequency harmonics such as 11th harmonic in this case at low switching frequency.

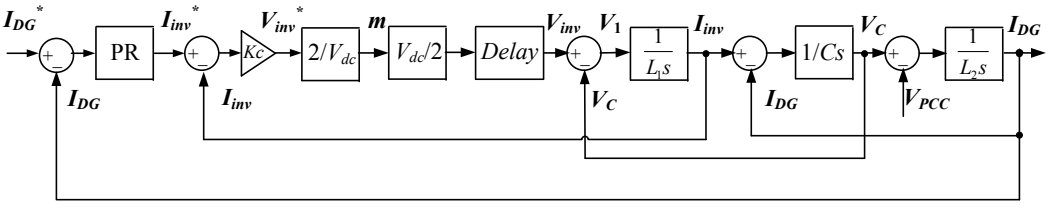

Fig. 1.9 Control scheme of the conventional CCM based method

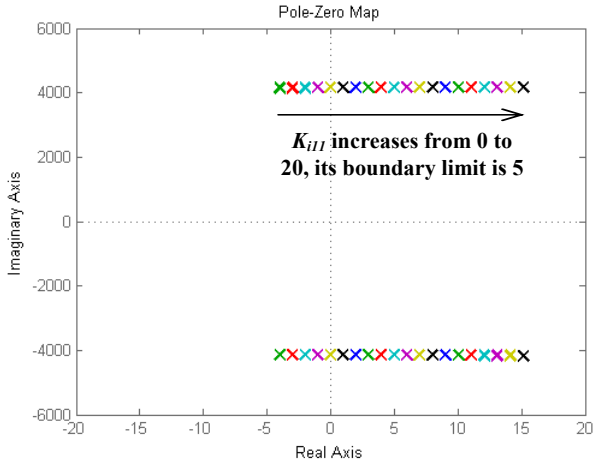

Fig. 1.10 Pole positions of I_{DG}/I_{DG}* with different 11th harmonic integral gain

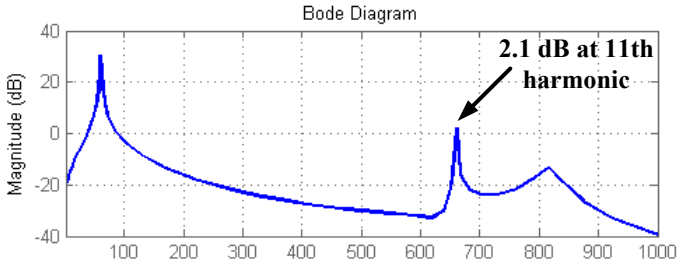

Fig. 1.11 Bode magnitude plot of the open loop transfer function using the maximum 11th harmonic integral gain

1.4 Research Objectives and Thesis Layout

As discussed above, compared with APFs, the relatively lower switching frequency and higher power rating of DG interfacing converter will limit the control bandwidth of the conventional harmonic compensation method, so the harmonics compensation will be challenging especially when compensating high frequency harmonics. To overcome this drawback, a harmonic compensation method using DG-grid interfacing converter at relatively low switching frequency is developed and discussed in the thesis.

In the rest of the thesis, Chapter 2 describes the harmonic control strategy of the proposed method. Then the simplified model of the single DG-grid system with the proposed harmonic compensation method and the corresponding full model of the system are established for further analysis. The simplified system model can be adopted to evaluate harmonic compensation performance for low frequency harmonics such as 5^{th} and 7^{th} harmonics since it is almost the same as the full system model for low frequency harmonics. When the DG unit equivalent impedance at harmonic frequencies is required to be controlled as specific impedance accurately, the full system model should be used.

In Chapter 3, the design of virtual impedance for the proposed method is discussed based on the analysis of system stability and steady-state harmonic compensation performance. The virtual impedance design approach which could provide best harmonic compensation performance and keep the system stable is presented.

The simulation and experimental verification results of the proposed harmonic compensation method are provided in Chapter 4.

Finally, Chapter 5 summarizes the conclusion of the thesis and suggests some future work.

Chapter 2

Proposed Harmonic Compensation Method Using DG at Low Switching Frequency

A distribution system harmonic compensation approach using DG-grid interfacing converter is proposed in this chapter. The proposed method adjusts the PWM reference signal directly instead of modifying current reference and therefore is not limited to the current control bandwidth. Using this method, high harmonics compensation bandwidth can be achieved for the low switching frequency DG unit. This chapter describes the control strategies including the fundamental component control and the principle of harmonic compensation at first. Then the system model of proposed harmonic compensation method is established and the harmonic compensation performance is analyzed.

2.1 Proposed Harmonic Compensation Method

This section describes the control strategy of the proposed harmonic compensation method. For the fundamental component, a multi-loop current controller is used for DG current regulation. For the harmonic component, the PCC harmonic voltage is extracted to produce harmonic compensation signal.

2.1.1 Fundamental component control

The block diagram of the proposed harmonic compensation method is shown in Fig. 2.1. The most widely used CCM based method is adopted to control the fundamental component. In the multi-loop controller, the PR controller is used as the outer DG current loop and the inverter output current tracking loop with a

proportional controller is added as the inner loop control, which is introduced previously in equation (1.1) and Fig. 1.5.

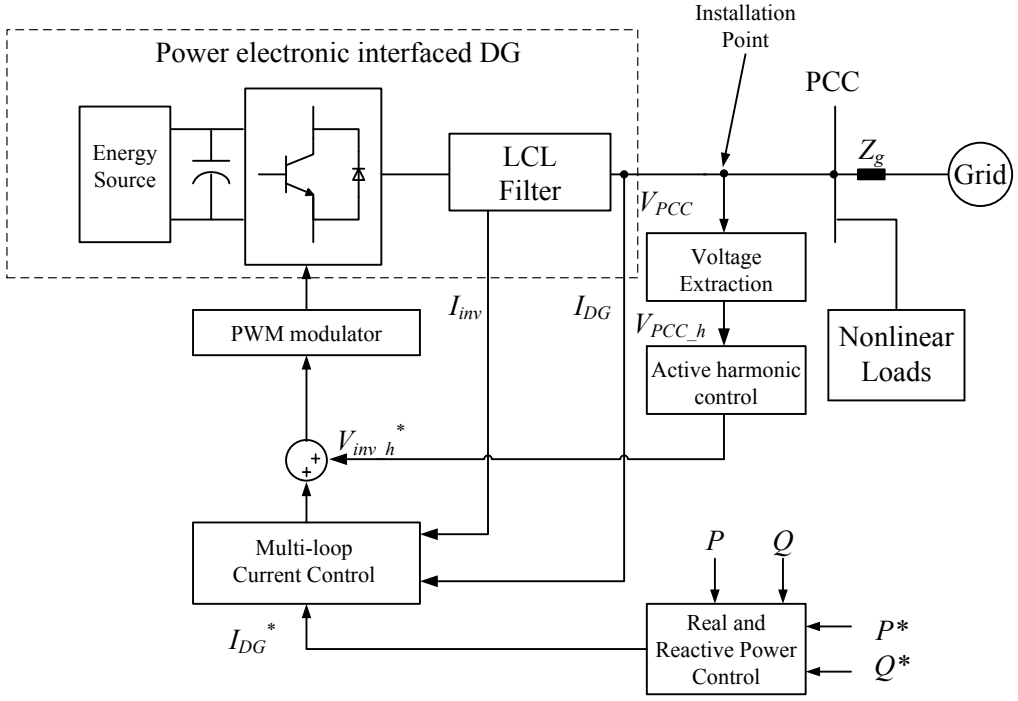

Fig. 2.1 Control strategy of the proposed harmonic compensation method

2.1.2 Principle of harmonic compensation

As the block diagram shown in Fig. 2.1, the extracted PCC harmonic voltage V_{PCC_h} is used to control the PWM reference signal directly instead of modifying the harmonic component of the reference current. Obviously, by avoiding the multi-loop control path, the harmonic compensation branch can be realized with a much higher bandwidth, meaning accurate compensation of relatively high order harmonics and better system stability. Moreover, the PR controller in the multi-loop current control scheme only needs to control the fundamental component which reduces the current control bandwidth requirement too. It is worthwhile to note that the voltage of PCC may be difficult to measure remotely under practical conditions. Therefore the installation point voltage can be measured as PCC voltage since they are close.

To extract the PCC harmonic voltage accurately with selective harmonic compensation, the notch filter is used, which is designed as:

$$SHD(s) = \frac{(h \cdot 120pi / Q_p)\mathrm{s}}{\mathrm{s}^2 + (h \cdot 120pi / Q_p)\mathrm{s} + (h \cdot 120pi)^2} \tag{2.1}$$

where h is harmonic order and Q_P is quality factor. Then the inverter output harmonic voltage V_{inv_h} is controlled by the extracted PCC harmonic voltage V_{PCC_h} as

$$V_{inv\_h} = -G \cdot V_{PCC\_h} \tag{2.2}$$

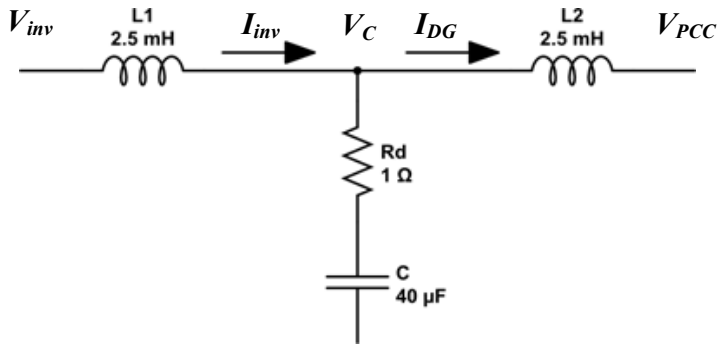

Fig. 2.2 Output LCL filter

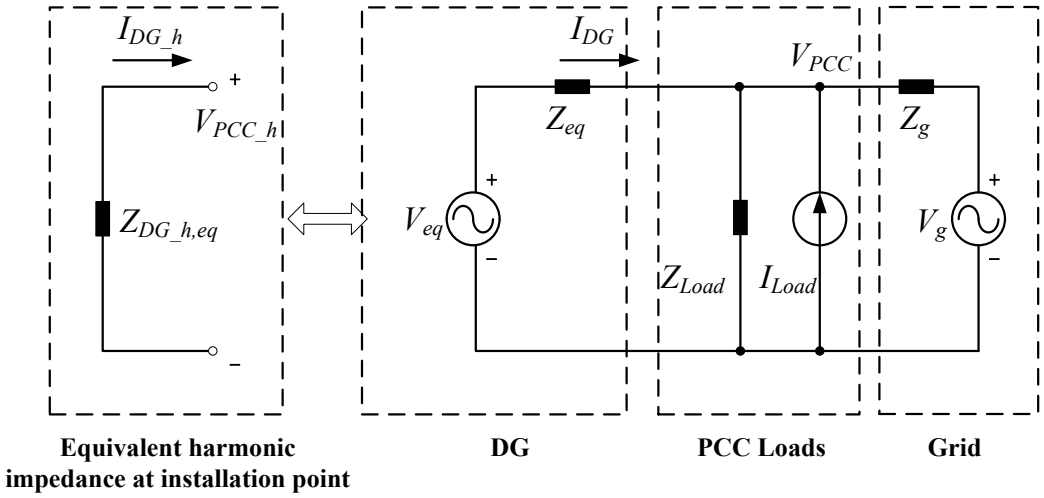

Fig. 2.3 Thevenin equivalent circuit of a single DG-grid system with the proposed compensation method

As the DG output voltage harmonics are not directly regulated, the Thevenin equivalent circuit of a single DG-grid system with LCL output filter as shown in Fig. 2.2 can be expressed as Fig. 2.3 for harmonic analysis. According to Thevenin's theorem, the DG unit is described as a voltage V_{eq} with output series impedance Z_{eq}

$$V_{eq} = V_{inv} \cdot \frac{Z_C}{Z_{L1} + Z_C} \tag{2.3}$$

$$Z_{eq} = \frac{Z_{L1}Z_{L2} + Z_{L1}Z_C + Z_{L2}Z_C}{Z_{L1} + Z_C} \tag{2.4}$$

where V_{inv} is the inverter output voltage, Z_{L1}, Z_{L2} and Z_C are the impedance of LCL filter. The PCC nonlinear load is represented as a passive load and harmonic current source, and the grid can be regarded as a voltage source V_g and grid impedance Z_g. Then the equivalent impedance of DG unit at harmonic frequencies can be obtained as

$$I_{DG\_h} = \frac{V_{eq\_h} - V_{PCC\_h}}{Z_{eq}} = -\frac{(G \cdot Z_C / (Z_{L1} + Z_C) + 1) \cdot V_{PCC\_h}}{Z_{eq}} \tag{2.5}$$

$$Z_{DG\_h,eq} = -\frac{V_{PCC\_h}}{I_{DG\_h}} = \frac{1}{G \cdot Z_C / (Z_{L1} + Z_C) + 1} \cdot Z_{eq} \tag{2.6}$$

It is can be seen that by controlling the inverter output harmonic voltage with a feedback gain G, the equivalent harmonic impedance of DG will be scaled down by a factor K which is defined as $[G \cdot Z_C / (Z_{L1}+Z_C)+1]$. When the factor K is set as 1, the system will be a standard CCM controlled DG unit without any harmonic control. When K is greater than 1, the PCC harmonic voltage will be reduced because the DG unit absorbs more harmonics due to the reduced equivalent impedance. This operation mode is defined as harmonics compensation in this work. When K is greater than 0 and less than 1, DG unit works in harmonic rejection mode. During harmonic rejection operation, the DG equivalent impedance increases at harmonic frequencies to reject harmonics so that the DG unit has lower harmonics and better THD to meet grid connection requirements.

For the single DG system whose parameters are same as Table 1.3 and the switching frequency is 2 kHz, the harmonic performances of the proposed method when compensating harmonics and rejecting harmonics in the simulations are shown in Fig. 2.4 and Fig. 2.5 respectively. It is can be seen that the THD of PCC voltage is reduced from 15.06% without harmonic compensation to 4.66% in Fig. 2.4. And when K is set as between 0 and 1 by selecting proper G, the PCC voltage and the grid current are distorted, leaving an improved DG current with lower THD as shown in Fig. 2.5. Therefore, the effectiveness of the proposed harmonic compensation method is verified preliminary. More simulation and experimental results will be presented in Chapter 4. Note that in this thesis, the focus is on system harmonics compensation using DG, and therefore the harmonics rejection operation will not be further discussed.

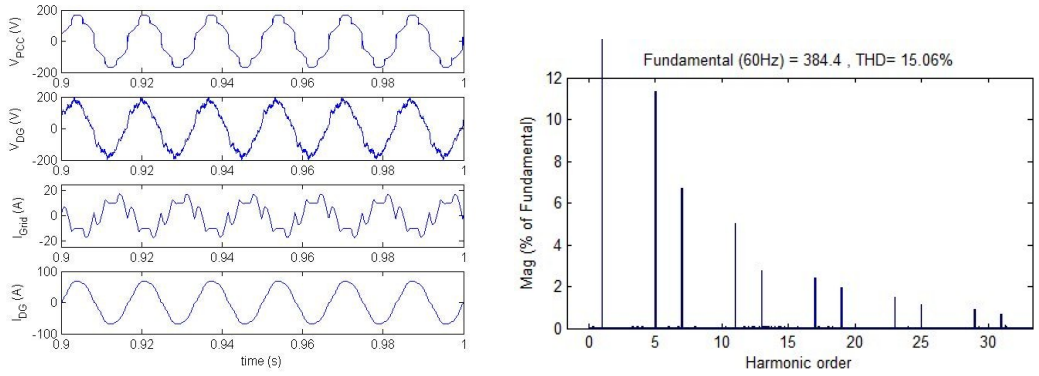

(a)

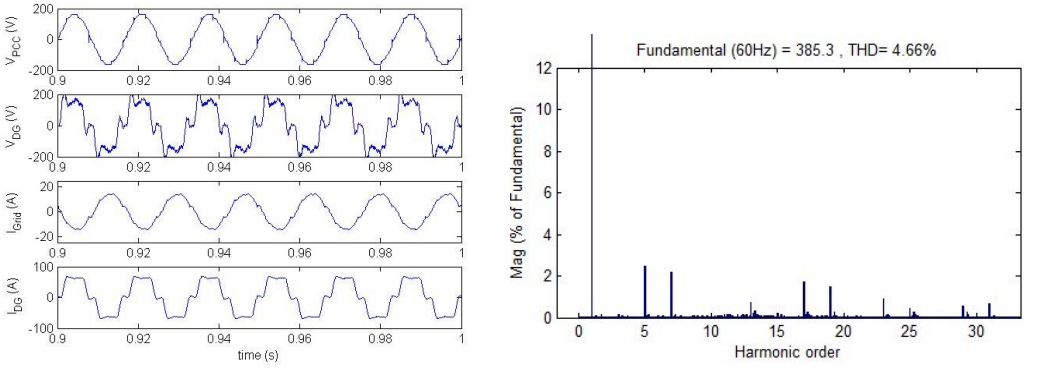

(b)

Fig. 2.4 Harmonic compensation performance of PCC voltage (P=20 kW, f_{sw}=2 kHz). (a) Without compensation. (b) Proposed harmonic compensation method.

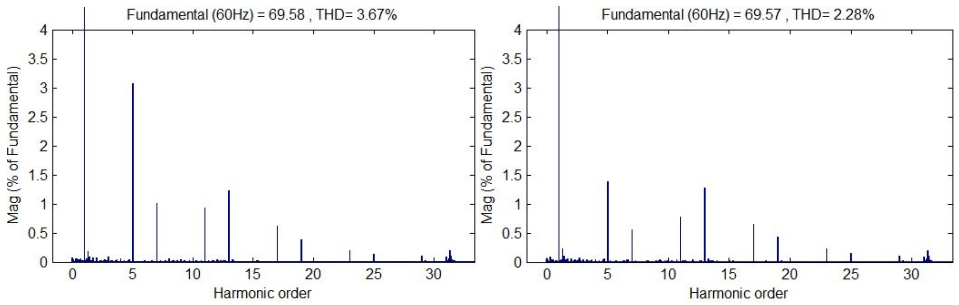

(a) (b)

Fig. 2.5 Harmonic analysis of DG current. (a) Without harmonic rejection. (b) Harmonic rejection.

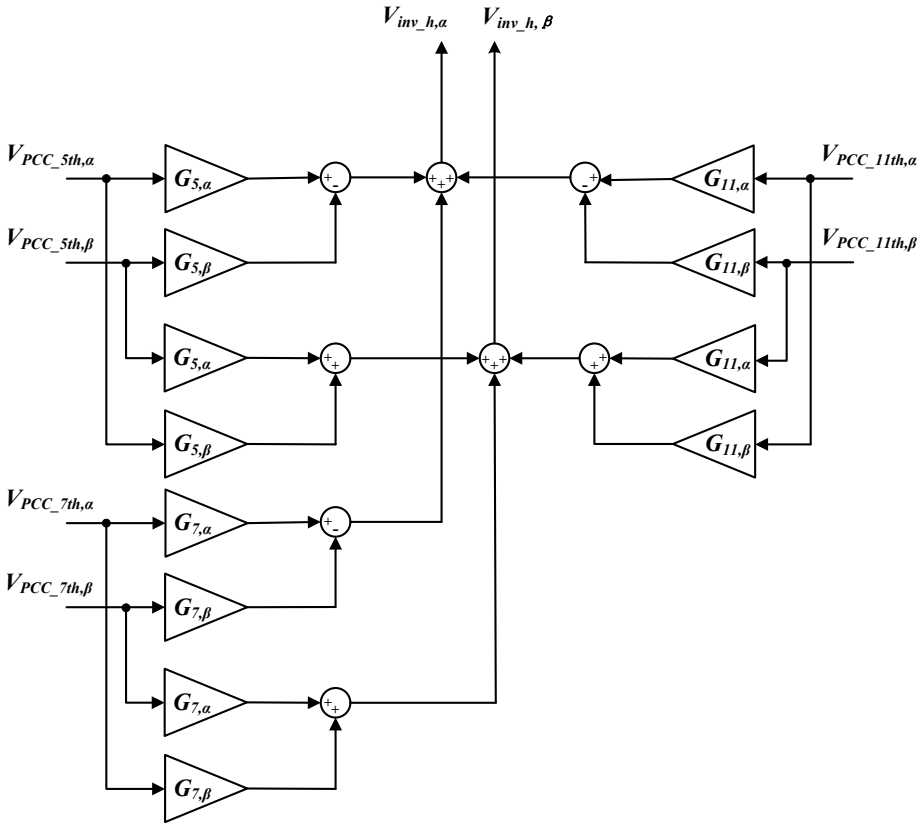

Fig. 2.6 Harmonic compensation signal generation in α-β frame

In addition, when the DG unit is working in a multiple DG system, the phase angle mismatch of harmonic impedance may introduce circulating current between DG units. Setting G as a proper complex number can make the equivalent harmonic impedance to be a resistance. As a result, all the DG units in the multiple DG system can operate as R-APF with minimum circulating current

and better damping to the system harmonics. The block diagram using a complex feedback gain G to generate compensation signal to compensate 5^{th}, 7^{th} and 11^{th} harmonics in α-β frame is shown in Fig. 2.6. In α-β frame, the harmonic feedback gain G can be transferred as a complex number ($G_{h,\alpha}+G_{h,\beta}\ i$) , and the extracted PCC harmonic voltage also can be regarded as ($V_{PCC\_h,\ \alpha}+V_{PCC\_h,\ \beta}\ i$). In order to obtain harmonic compensation signal, the corresponding G and extracted PCC harmonic voltage are multiplied together, then the harmonic compensation signals for different harmonics are combined to get the final harmonic compensation signal.

However, the harmonic impedances introduced by the multi-loop controller are not taken into account in equations both (2.5) and (2.6). The equivalent impedance of DG unit in equation (2.6) is an approximation. If the gain of multi-loop controller is not small enough at harmonic frequencies, it may have an impact on harmonic compensation performance. In the next section, both the simplified system model without considering the controller introduced impedance and the full system model are established for further analysis.

2.2 Analysis of Proposed Control Strategy

In this section, the simplified model of the single DG-grid system with the proposed harmonic compensation method and the corresponding full system model are established. Then the theoretical harmonic compensation performances using simplified model and full model are provided and analyzed. The practicability of simplified model is studied.

2.2.1 Simplified and full system models

According to the LCL filter shown in Fig. 2.2, equations (2.7), (2.8) and (2.9) can be obtained as

$$V_{inv} - V_C = \mathrm{s}L_1 I_{inv} \tag{2.7}$$

$$V_C - V_{pcc} = \mathrm{s}L_2 I_{DG} \tag{2.8}$$

$$I_{DG} = I_{inv} - \frac{V_C}{R_d + \frac{1}{\mathrm{s}C}} \tag{2.9}$$

where R_d is a damping resistor connected in series with the capacitor. Based on the equations (2.7), (2.8) and (2.9), the DG current I_{DG} and the inverter output current I_{inv} can be expressed as

$$I_{DG} = (V_{inv} - H_1 \cdot V_{pcc}) \cdot H_2 \tag{2.10}$$

$$I_{inv} = H_3 \cdot I_{DG} + H_4 \cdot V_{pcc} \tag{2.11}$$

where

$$H_1 = \frac{\mathrm{s}^2 C L_1 + \mathrm{s}R_d C + 1}{\mathrm{s}R_d C + 1}$$

$$H_2 = \frac{\mathrm{s}R_d C + 1}{\mathrm{s}^3 C L_1 L_2 + \mathrm{s}^2 R_d C (L_1 + L_2) + \mathrm{s}(L_1 + L_2)}$$

$$H_3 = \frac{\mathrm{s}^2 C L_2 + \mathrm{s}R_d C + 1}{\mathrm{s}R_d C + 1}$$

$$H_4 = \frac{\mathrm{s}C}{\mathrm{s}R_d C + 1}$$

The control scheme for the single DG-grid system using the proposed harmonic compensation method is shown in Fig. 2.7. When the harmonics that pass through the PR controller and the grid voltage harmonics are small enough, Fig. 2.7 can be simplified to Fig. 2.8 at harmonic frequencies

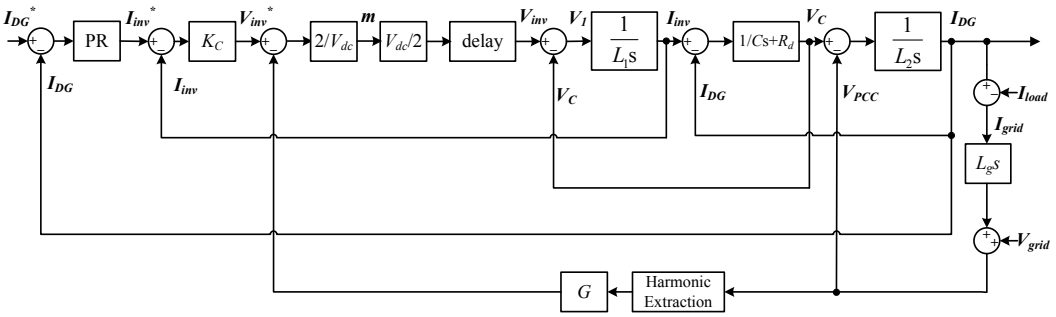

Fig. 2.7 Control scheme for the single DG-grid system using the proposed harmonic compensation method

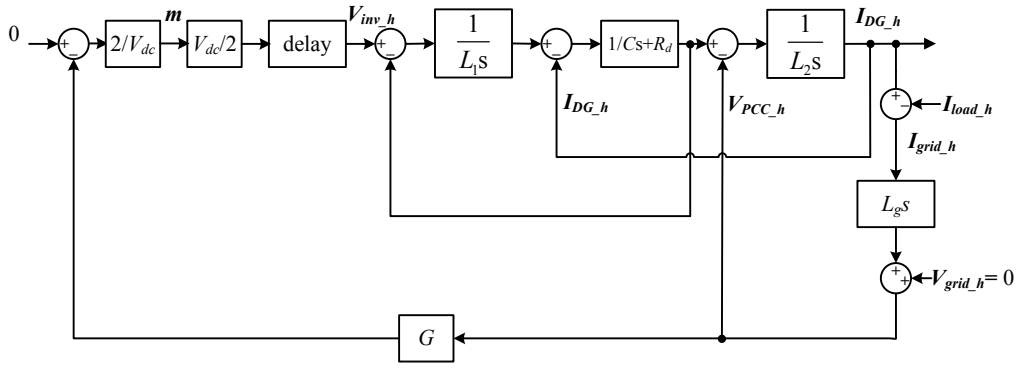

Fig. 2.8 Simplified control scheme for the single DG-grid system using the proposed harmonic compensation method

According to equations (2.10), (2.11) and Fig. 2.8, the equivalent impedance of DG unit at harmonic frequencies can be obtained as

$$\begin{aligned} Z_{DG\_h,eq} &= -\frac{V_{PCC\_h}}{I_{DG\_h}} = \frac{1}{H_2(G+H_1)} \\ &= \frac{s^3 CL_1L_2 + s^2 R_d C(L_1+L_2) + s(L_1+L_2)}{s^2 CL_1 + sR_d C + 1 + G(sR_d C + 1)} \end{aligned} \tag{2.13}$$

where G is the harmonic compensation feedback gain, H_1 and H_2 are the equations derived above. Based on equation (2.6), the equivalent impedance of DG unit can also be obtained as

$$
\begin{aligned}
Z_{DG\_h,eq} &= \frac{1}{G \cdot Z_C / (Z_{L1} + Z_C) + 1} \cdot Z_{eq} \\
&= \frac{Z_{L1}Z_{L2} + Z_{L1}Z_C + Z_{L2}Z_C}{GZ_C + Z_{L1} + Z_C} \\
&= \frac{\mathrm{s}^3 CL_1L_2 + \mathrm{s}^2 R_d C(L_1 + L_2) + \mathrm{s}(L_1 + L_2)}{\mathrm{s}^2 CL_1 + \mathrm{s}R_d C + 1 + G(\mathrm{s}R_d C + 1)}
\end{aligned}
\tag{2.14}
$$

It can be observed that equations (2.13) and (2.14) are exactly the same, which confirms the feasibility of the simplified system model.

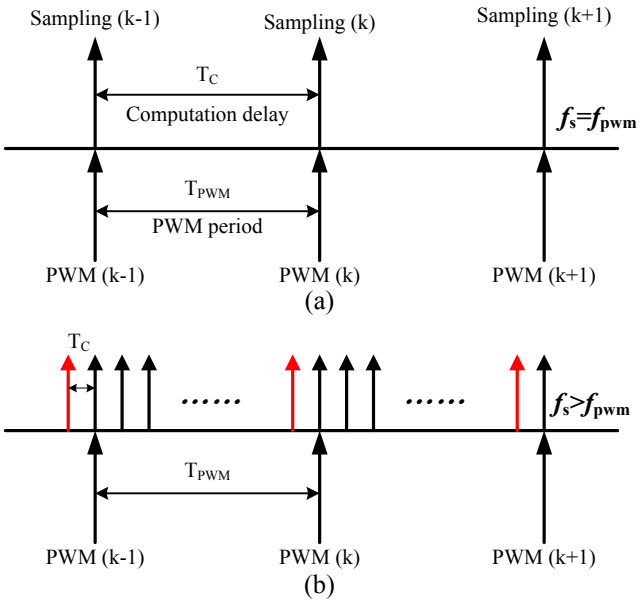

Fig. 2.9 Delay mechanism. (a) Sampling frequency is same as PWM frequency. (b) Sampling frequency is much higher than PWM frequency

In addition, since the proposed harmonic control method is applied at low frequencies, the switching delay produced during modulation in digital control should be taken into account in practice. The delay mechanism is shown in Fig. 2.9 in which the delay consists of two components: computation delay and PWM delay [37]. Considering the fact that the switching frequency of the proposed method is low, multisampling is applied to the proposed method to reduce the computation delay T_C, as shown in Fig. 2.9 (b). As a result, when the sampling

frequency f_s is much higher than PWM frequency f_{PWM}, the computation delay T_C is negligibly small (f_s=10 f_{PWM} in this work).

On the other hand, since the PWM reference is needed to hold on and compared to the triangular carrier to generate modulation signal after the PWM reference is update. This behavior introduces PWM delay and it is can be expressed as a zero-order hold (ZOH) [37], which is defined as

$$H_{ZOH}(s) = \frac{1 - e^{-sT_{PWM}}}{s} \tag{2.15}$$

The equation H_{ZOH} (s) is approximately equal to $T_{PWM}e^{-0.5sT_{PWM}}$ when $s = j\omega$ applied, which introduces the PWM delay that is equal to $0.5T_{PWM}$. Therefore, when multisampling is applied, the delay of proposed method is approximately equal to half PWM period. In this work, the second-order Pade approximation which is a rational function is used to approximate the delay in the calculation. Therefore, the equation (2.13) can be rewritten as

$$Z_{DG\_h,eq} = -\frac{V_{PCC\_h}}{I_{DG\_h}} = \frac{1}{H_2(G \cdot D + H_1)} \tag{2.16}$$

where D is the transfer function of the switching delay. In addition, as mentioned previously, the equivalent harmonic impedance $Z_{DG\_h,eq}$ can be controlled to be a virtual resistance R_h by setting G as a proper complex number to provide better damping to the system. For the virtual resistance R_h, the corresponding complex number G can be obtained as

$$G = \frac{1 - H_1 H_2 R_h}{H_2 R_h D} \tag{2.17}$$

To further evaluate the harmonic compensation performance under different parameter conditions, the attenuation between grid harmonic current I_{grid_h} and nonlinear load harmonic current I_{load_h} ($|I_{grid\_h}/I_{load\_h}|$) is used to show how much harmonic current flows from nonlinear load into the grid. In the simplified system model, the relationship between I_{grid_h} and I_{load_h} can be obtained as

$$\frac{I_{grid\_h}}{I_{load\_h}} = \frac{1}{-H_2 \cdot sL_g(G \cdot D + H_1) - 1} \tag{2.18}$$

Since neglecting the harmonics that pass through the controller may lead to an impact on harmonic compensation performance, the full system model also needs to be established. According to Fig. 2.7, the DG unit equivalent impedance at harmonic frequencies in the full system model can be expressed as

$$Z_{DG\_h,eq} = -\frac{V_{PCC\_h}}{I_{DG\_h}} = \frac{1+K_C H_2 D \cdot PR + K_C H_2 H_3 D}{K_C H_2 H_4 D + H_1 H_2 + H_2 G \cdot D} \tag{2.19}$$

where PR is the transfer function of PR controller, K_C is the proportional gain of the inner loop control, G is the harmonic compensation feedback gain, D is switching delay, H_1 to H_4 are the transfer functions as described previously. The attenuation between grid harmonic current I_{grid_h} and nonlinear load harmonic current I_{load_h} in the full system model can be obtained as

$$\frac{I_{grid\_h}}{I_{load\_h}} = \frac{-H_2 K_C D(PR + H_3) - 1}{1 + H_2 \mathrm{s}L_g(G \cdot D + H_1) + H_2 K_C D(PR + H_3 + \mathrm{s}L_g H_4)} \tag{2.20}$$

In addition, when the equivalent harmonic impedance $Z_{DG\_h,eq}$ is controlled to be a resistance R_h, the complex number G can be obtained as

$$G = \frac{1 + K_C H_2 D \cdot PR + K_C H_2 H_3 D - K_C H_2 H_4 R_h D - H_1 H_2 R_h}{H_2 R_h D} \tag{2.21}$$

2.2.2 Analysis of simplified and full system models

To begin with, the effectiveness of the simplified model and the full model will be discussed when the harmonic compensation feedback gain G is set as a real number. The parameters of the single DG-grid system in the theoretical

analysis are the same with the ones in the experiments and listed in Table 4.1 in Chapter 4.

Fig. 2.10 shows the steady-state 5th harmonic compensation performances (attenuation=$|I_{grid\_h}/I_{load\_h}|$) using the simplified model and full model when real number 5th harmonic feedback gain G_5 increases from 0 to 68. In Fig. 2.10, Y-axis is the attenuation gain $|I_{grid\_h}/I_{load\_h}|$, X-axis is the value of G_5, the dotted line represents the simplified model, and the solid line represents the full model. This range of G_5 is determined by the system stability. The issue about system stability and harmonic compensation feedback gain G design will be discussed in detail in Chapter 3. In this part, we put emphasis upon the steady-state harmonic compensation performances of the simplified model and full model. It can be seen in Fig. 2.10 that the 5th harmonic compensation performances of simplified model and full model are almost the same, especially when G_5 is set as a relatively large real number.

Similarly, the steady-state compensation performances using the simplified model and full model for 7th and 11th harmonics are shown in Fig. 2.11 and Fig. 2.12 respectively. As shown in Fig. 2.11, when G_7 is large enough, the simplified model also can be seen equivalent to the full model. However, there is a certain error between simplified and full models for 11th harmonic in Fig. 2.12. This error is more obvious when the compensation gain G_{11} is small. Therefore, when the accurate DG unit equivalent impedance is not required strictly and the harmonic frequency is relatively low such as 5th and 7th harmonics, the simplified model can be used for evaluating the proposed method.

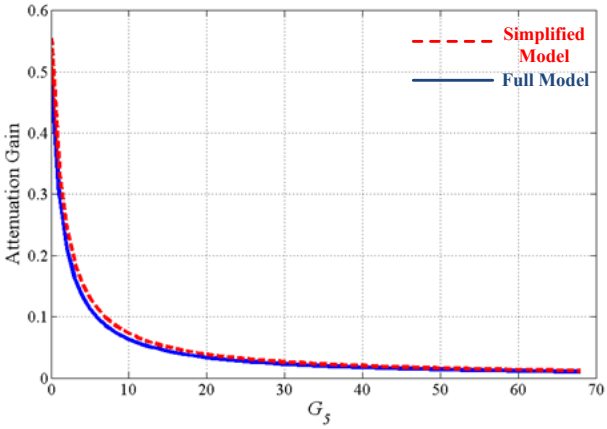

Fig. 2.10 Steady-state compensation performance for 5th harmonic (G_5 ranges from 0 to 68)

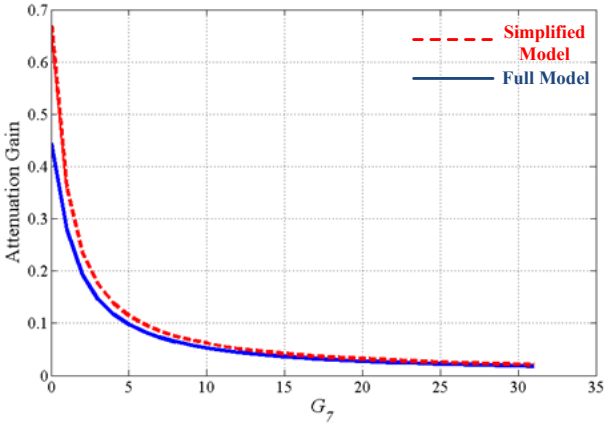

Fig. 2.11 Steady-state compensation performance for 7th harmonic (G_7 ranges from 0 to 31)

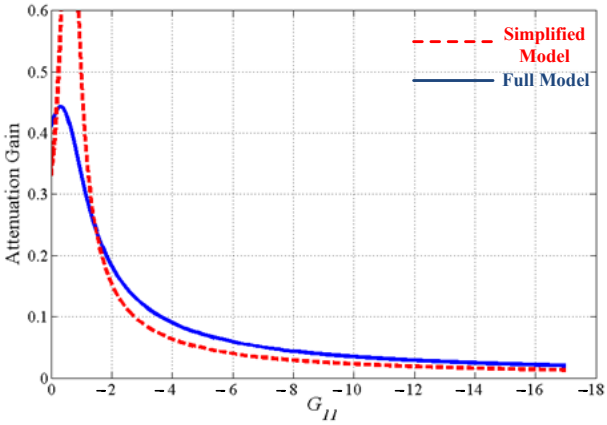

Fig. 2.12 Steady-state compensation performance for 11th harmonic (G_{11} ranges from 0 to -17)

In addition, the effectiveness of the simplified model when the DG equivalent impedance is controlled to be a virtual resistance by a proper complex G will be discussed. When the virtual resistance R_h at harmonic frequency is set as 0.5 ohm, the corresponding G_h of the simplified and full model are shown in Table 2.1. It can be observed that the G_h in the simplified model has a certain amount of error on both the amplitude and phase angle. As a result, when the compensation gain is designed through the simplified model, the actual virtual impedance presented by DG may not be an accurate resistance. Thus the simplified model should not be applied when accurate virtual impedance is required.

Table 2.1 Corresponding G_h when the virtual impedance is controlled as a resistance in simplified and full models

	5^{th}	7^{th}	11^{th}
R_h (ohm)	0.5	0.5	0.5
G_h (simplified model)	15.52∠120.31	17.28∠132.01	8.24∠187.38
G_h (full model)	12.74∠89.51	14.46∠118.96	13.56∠177.18

2.3 Summary

This chapter introduces a distribution system harmonic compensation approach using DG-grid interfacing converter at low switching frequency. Although the conventional compensation method has a good compensation performance at high switching frequency, it is not effective at low switching frequency which is expected for high power DG-grid interfacing converters to reduce switching losses. The proposed method adjusts the PWM reference signal directly instead of modifying current reference, thus it can achieve the effective high order harmonic compensation at a relatively low switching frequency. The control strategies including fundamental component control and principle of harmonic compensation are discussed at first. The proposed method can be used for either distribution system harmonic compensation or for reduction of the DG

output current harmonics. And if controlled properly, the DG unit can also act as a virtual resistance to provide damping to the system.

In order to further analyze the proposed method, both the simplified and the full system models are established. The harmonic impedance introduced by the controller is not considered in the simplified model. Compared with the full model, the simplified model is intuitively clearer and easier to calculate. When the harmonic compensation gain G is set as a relatively large real number, the simplified model is equivalent to the full model for low order harmonics such as 5^{th} and 7^{th} harmonics. On the other hand, the full system model can provide accurate date for analysis and harmonic compensation gain design. When a virtual resistance or specific virtual impedance is required, the full system model should be applied.

Chapter 3

Design of Virtual Impedance for Harmonics Compensation

As mentioned in the previous chapter, by setting proper amplitude and phase angle of the harmonic compensation gain G, the equivalent impedance of the DG unit can be controlled to be a specific impedance (resistive, inductive or capacitive). For a real number G, the proposed method is easier to implement. For a proper complex number G which makes the DG unit equivalent impedance a resistance, the proposed method has the potential to provide additional damping to the system. This chapter investigates how to design the virtual impedance to get a satisfactory harmonics compensation performance. To begin with, the system stability is analyzed when G is under different phase angles. Then the system stability and compensation performance are analyzed when three different virtual impedance design schemes: virtual impedance using a real number harmonic compensation gain G, virtual resistance using a proper complex number G, and virtual impedance using the complex number G whose phase angle is set as the angle that provides optimal compensation performance when the modulus of G is fixed. It is shown that the real number G can provide better harmonic compensation performance at relatively low switching frequency due to the better system stability.

3.1 System Stability Analysis

As discussed in the previously chapter, according to equation (2.6) in the simplified system model and equation (2.19) in the full system model, it can be seen that the equivalent harmonic impedance of DG is scaled down by a factor which contains harmonic compensation gain G. The larger the modulus of G with

a proper phase angle, the smaller the corresponding equivalent harmonic impedance. As a result, more harmonics introduced by nonlinear load are absorbed by the DG unit, and the grid current will be more distortion-free leading to better PCC voltage quality. This section investigates how the harmonic compensation gain G affects the system stability. Obviously the larger modulus of G will reduce the stability margin, and therefore the focus in this section is to investigate how the phase angle of G affects the stability.

With the control scheme for the single DG-grid system using the proposed harmonic compensation method in Fig. 2.7, the transfer function of the system can be obtained as

$$\frac{I_{DG}}{I_{DG}^{*}} = \frac{H_2 PR \cdot K_C D}{1 + H_2 Z_g (G \cdot SHD \cdot D + H_1) + H_2 K_C D(PR + H_3 + H_4 Z_g)} \tag{3.1}$$

where PR is the transfer function of PR controller, K_C is the proportional gain of the inner loop control, G is the harmonic compensation feedback gain, D is switching delay, H_1 to H_4 are the transfer functions as described previously, Z_g is the transfer function of grid impedance which is defined as L_gs, and SHD is harmonic extraction block.

Based on equation (3.1), Fig. 3.1 shows the pole positions of the control scheme when the modulus of 5th harmonic compensation feedback gain G_5 is set as a constant ($|G_5|$=5) with different phase angles. The pole positions of the control scheme are calculated every degree in the theoretical analysis, but they are marked every 45 degree in Fig. 3.1 in order to facilitate the observation. The parameters of the single DG-grid system are same as Table 4.1 in Chapter 4. As shown in Fig. 3.1, with the phase angle of G_5 increasing, the pair of poles closest to the right half plane move anticlockwise, and become an oval finally. According to the obtained pole positions, when the phase angle of G_5 is 0 degree, this pair of poles is farthest away from the imaginary axis in the left half plane, which means the system is the most stable at this time. And Table 3.1 shows the modulus range of G_5 that makes the system stable under different phase angles. It is can be seen

that with the phase angle of G_5 increasing from 0, the system stability deteriorates quickly. And the modulus range when phase angle is 0 degree is much greater than the other phase angles. In conclusion, the system has better stability when G_5 is a real number without changing harmonic compensation signal phase angle.

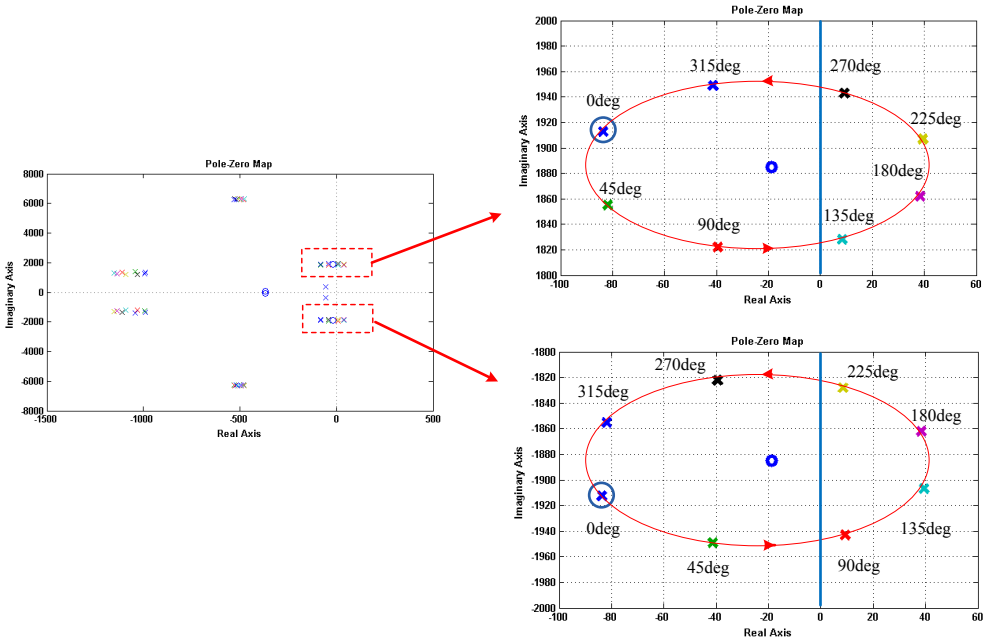

Fig. 3.1 Pole positions when compensating 5th harmonic under different phase angles ($|G_5|$=5)

Table 3.1 Modulus range of G_5 under different phase angles

Degree	0	45	90	135	180	225	270	315
Modulus range	68	35	3	1	1	1	3	35

Similarly, the pole positions of the control scheme when compensating 5th and 7th harmonics under the different G phase angles are shown in Fig. 3.2 and Fig. 3.3 respectively. The modulus ranges of G_7 and G_{11} under different phase angles are shown in Table 3.2 and Table 3.3 respectively. Likewise, the most stable phase angle for G_7 is also 0 degree based on Fig. 3.2 and the corresponding calculation results. However, the most stable phase angle for G_{11} is 180 degree. It is because that when the phase angle of G_{11} is set as 0 degree, the 11th harmonic

equivalent impedance of DG unit is calculated to be an impedance which contains negative resistance according to equation (2.19) in the full system model. The negative resistance has no physical meaning and tends to make the system unstable. Therefore, when G is a real number whose phase angle is 0 degree or 180 degree, the system stability is better than the one when G is a complex number. And 0 degree or 180 degree, which is the most stable phase angle can be determined by equation (2.19) by checking if the harmonic equivalent impedance contains negative resistance. In addition, the sign of G can also be determined easily by the equation (2.6) in the simplified system model. Since the harmonic equivalent impedance is scaled by a factor $[G \bullet Z_C / (Z_{L1}+Z_C) +1]$, G and $[Z_C / (Z_{L1}+Z_C)]$ need to be both positive/negative.

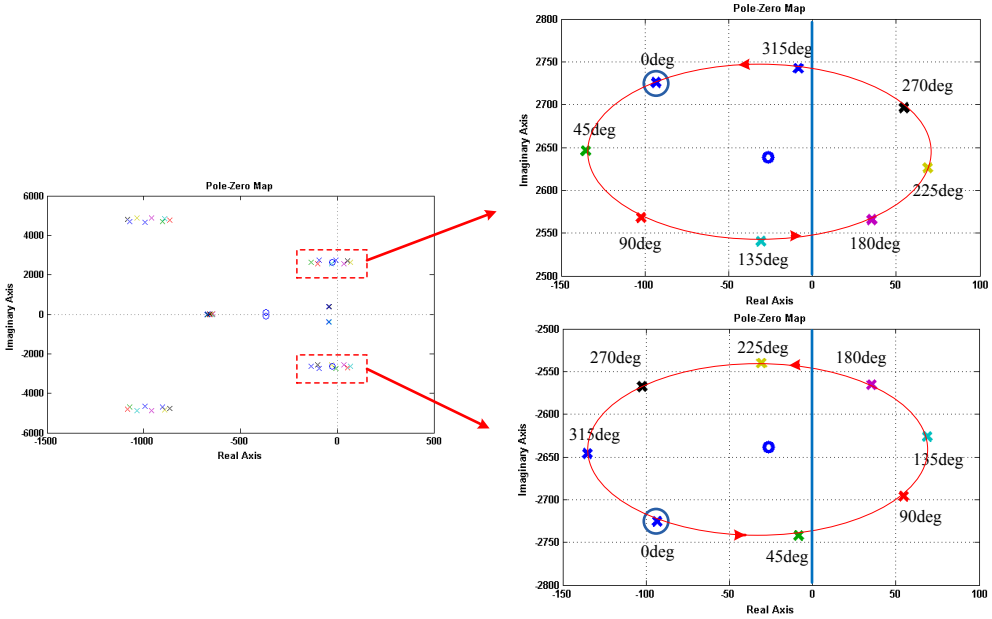

Fig. 3.2 Pole positions when compensating 7th harmonic under different phase angles ($|G_7|$=5)

Table 3.2 Modulus range of G_7 under different phase angles

Degree	0	45	90	135	180	225	270	315
Modulus range	31	5	1	1	2	1	1	5

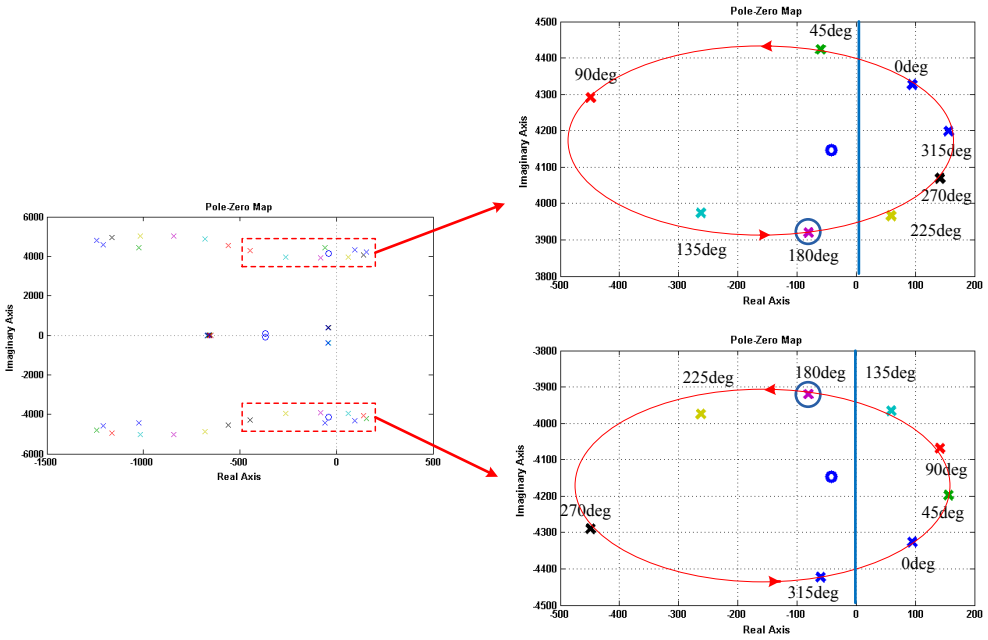

Fig. 3.3 Pole positions when compensating 11th harmonic under different phase angles ($|G_{11}|$=5)

Table 3.3 Modulus range of G_{11} under different phase angles

Degree	0	45	90	135	180	225	270	315
Modulus range	1	1	1	2	17	2	1	1

3.2 Virtual Impedance Design

This section describes the virtual impedance design of the proposed method. Through the discussion in the previous section, we know that the proposed harmonic compensation method using a real number harmonic feedback gain is not only easy to implement but also has better system stability than using a complex number harmonic feedback gain. Therefore, using real number G without changing harmonic compensation signal phase angle can be regarded as a suitable solution to design the equivalent virtual impedance. Thus the range of

real number G that makes the system stable and the corresponding harmonic compensation performance is analyzed at first in this section.

On the other hand, when the DG unit is working in a multiple DG system, the phase angle mismatch of harmonic impedance may introduce circuiting current between DG units. When the DG equivalent impedance is designed to be a virtual resistance, all the DG units in the multiple DG system can operate as R-APF with minimum circulating current and provide additional damping to the system harmonics. Therefore, the range of virtual resistance that makes the system stable and the corresponding harmonic compensation performance is also analyzed in this section to verify the feasibility of virtual resistance. What's more, when the modulus of G is fixed with different phase angles, the phase angle that provides optimal harmonic compensation performance can be obtained. And this optimal phase angle changes little with the modulus of G. Thus the effectiveness of the complex number G whose phase angle is set as its optimal phase angle is also discussed.

3.2.1 Virtual impedance using real number *G*

Fig. 3.4 shows the pole positions of the control scheme when real number G_5 is increased from 0 to 70. The G_5 maximum modulus that makes the system stable is 68. Fig. 3.5 shows the pole positions when real number G_7 is increased from 0 to 35 and the G_7 maximum modulus is 31. And the pole positions when real number G_{11} is decreased from 0 to -20 are shown in Fig. 3.6, in which the G_{11} maximum modulus is 17. According to equation (2.20), the harmonic compensation performances when the modulus of real number G is set as its maximum value are obtained and shown in Table 3.4. It is can be observed that the compensation performance is very effective because the good system stability allows the modulus of G to be set as a relatively large value.

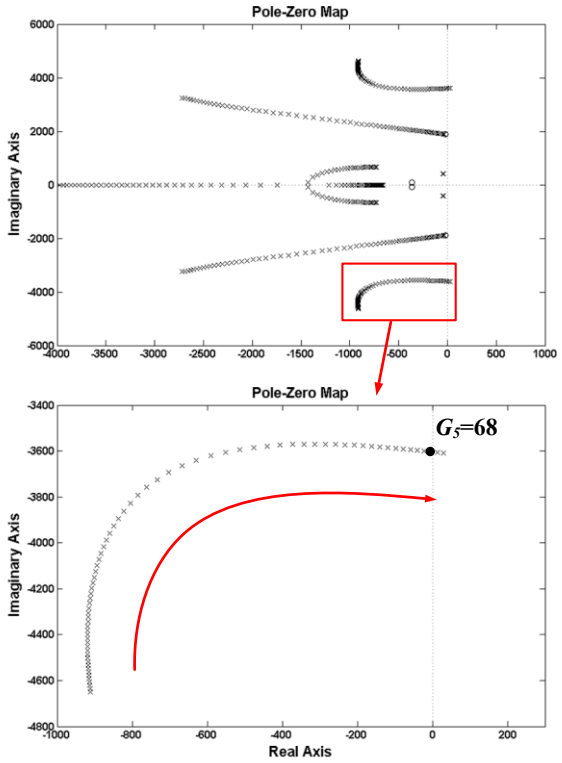

Fig. 3.4 Pole positions when real number G_5 is increased from 0 to 70

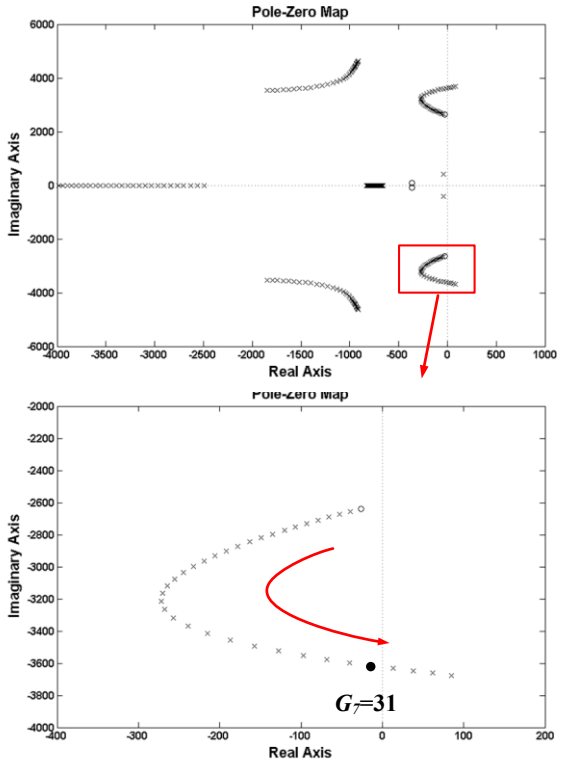

Fig. 3.5 Pole positions when real number G_7 is increased from 0 to 35

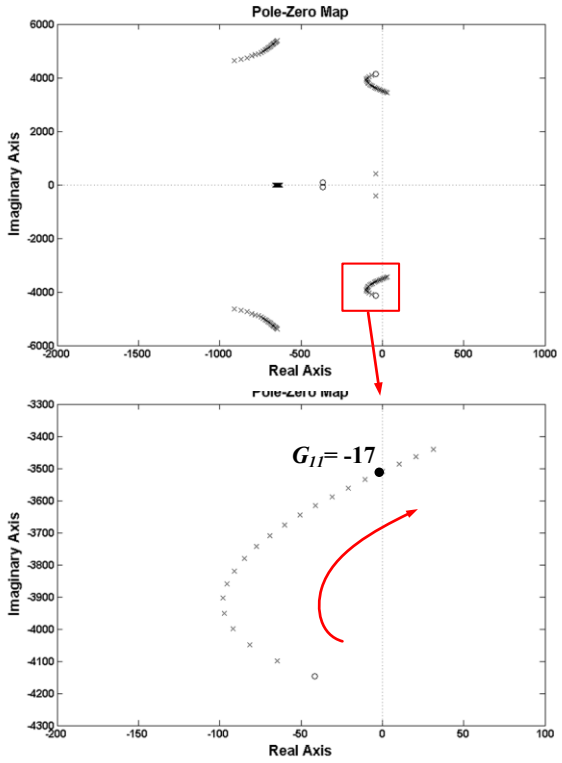

Fig. 3.6 Pole positions when real number G_{11} is decreased from 0 to -20

Table 3.4 Harmonic compensation performance when the modulus of real number G is set as its maximum value

	5th	7th	11th
G maximum modulus	68 (G_5=68∠0)	31 (G_7=31∠0)	17 (G_{11}=17∠180)
Attenuation ($\lvert I_{grid\_h}/I_{load\_h}\rvert$)	0.010	0.018	0.019

3.2.2 Virtual resistance

The feasibility of virtual resistance will be discussed in this section. To begin with, the ranges of virtual resistance R_h that ensures the system stability are provided. As we know, with the decrease of virtual resistance, the amplitude of the corresponding G increases and the system stability gets worse. Fig. 3.7 shows

the pole positions of the control scheme when the virtual resistance at 5th harmonic frequency R_5 is decreased from 4 Ω to 1 Ω. The minimum R_5 that makes the system stable is 2.3 Ω. Fig. 3.8 shows the pole positions when the virtual resistance at 7th harmonic frequency R_7 is decreased from 6 Ω to 3 Ω, and the minimum R_7 that makes the system stable is 4.4 Ω. Fig. 3.9 shows the pole positions when the virtual resistance at 11th harmonic frequency R_{11} is decreased from 3 Ω to 0.1 Ω, and the minimum R_{11} that makes the system stable is 0.5 Ω.

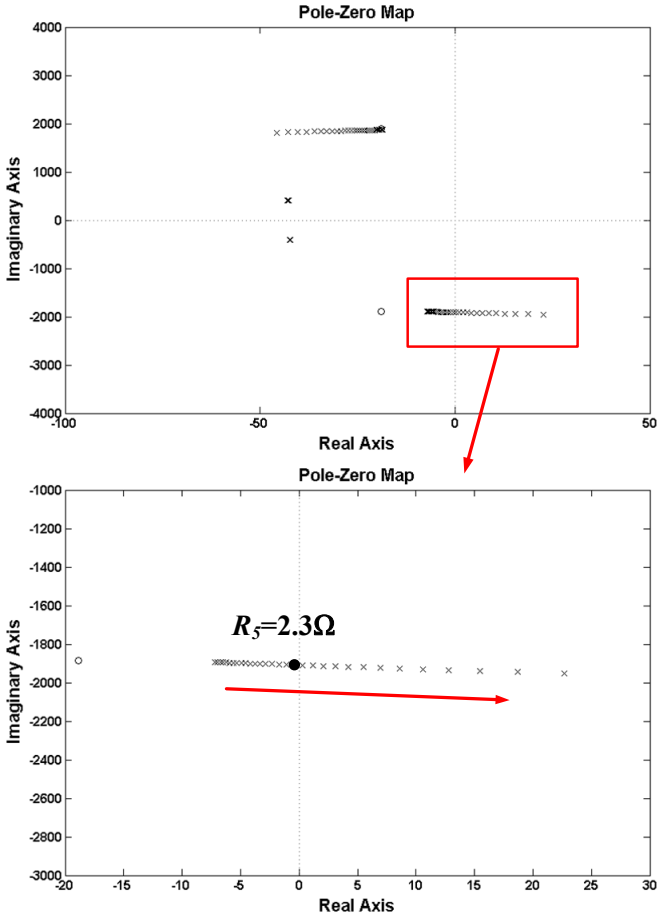

Fig. 3.7 Pole positions when virtual resistance R_5 is decreased from 4 Ω to 1 Ω

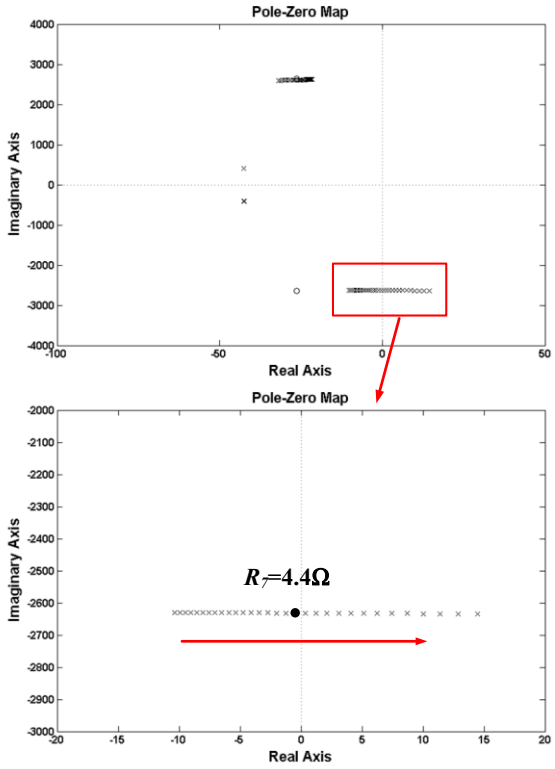

Fig. 3.8 Pole positions when virtual resistance R_7 is decreased from 6 Ω to 3 Ω

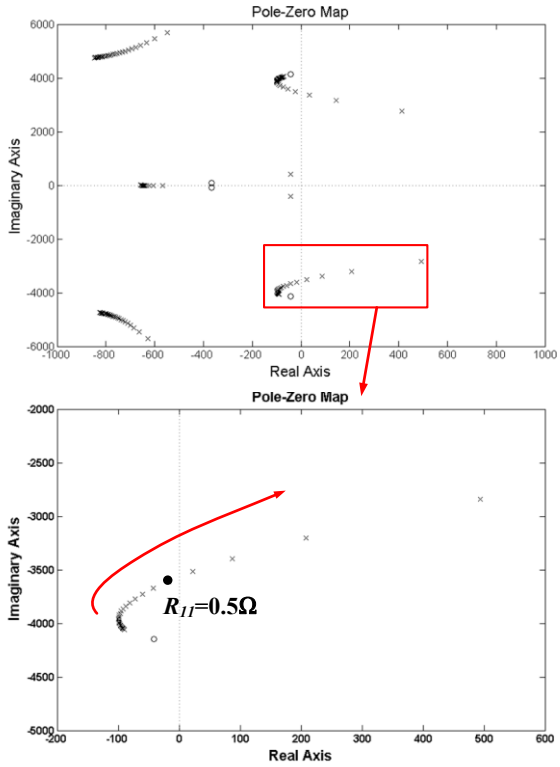

Fig. 3.9 Pole positions when virtual resistance R_{11} is decreased from 3 Ω to 0.1 Ω

Table 3.5 Harmonic compensation performance when the virtual resistance at harmonic frequency is set as its minimum value

	5th	7th	11th
Minimum R_h	2.3 Ω (G_5=2.27∠101.2)	4.4 Ω (G_7=1.27∠143.6)	0.5 Ω (G_{11}=13.56∠177.2)
Attenuation ($\lvert I_{grid\_h}/I_{load\_h}\rvert$)	0.237	0.317	0.024

Then the corresponding harmonic compensation performances when the virtual resistance R_5, R_7 and R_{11} are controlled to be their minimum values are shown in Table 3.5. Compared with Table 3.4, the harmonic compensation performances using virtual resistance are much worse than the ones using real number G at 5^{th} and 7^{th} harmonics. The compensation performances at 11^{th} harmonic are similar. It is because the phase angles of G_5 and G_7 when the virtual resistance is applied are too far away from their most stable angle (0 degree), so that their compensation performances are limited by poor system stability. But the phase angle of G_{11} when using virtual resistance is very close to its most stable angle (180 degree), thus the virtual resistance at 11^{th} harmonic can achieve an effective compensation performance. However, the phase angle corresponded to virtual resistance is determined by grid, DG unit, switching delay and controller together, which is hard to control through the virtual impedance design. It is worthwhile to note that when the switching frequency is increased, the system stability using virtual resistance will be greatly improved due to the reduced switching delay. In conclusion, virtual resistance is not flexible for the proposed harmonic compensation method at relatively low switching frequency.

3.2.3 Virtual impedance using complex number *G*

When the modulus of G is fixed, the G phase angle that provides optimal harmonic compensation performance can be obtained. Therefore, the feasibility of virtual impedance using the complex number G which provides optimal harmonic

compensation performance when its modulus is a constant will be discussed in this section.

Fig. 3.10 shows the steady-state compensation performance for 5th harmonic when $|G_5|$ = 5, 7 and 15. The X-axis is the phase angle of G_5 and the Y- axis is the attenuation gain $|I_{grid\_h}/I_{load\_h}|$ which reflects the 5th harmonic compensation performance. The three lines represent $|G_5|$ = 5, 7 and 11 respectively. Based on Fig. 3.10 and the corresponding calculation results, when the modulus of G_5 is set as 5, the phase angle that provides the minimum attenuation gain is 27 degree. As the modulus of G_5 increased, the phase angle that provides the minimum attenuation gain changes little as shown in Fig. 3.10. As a result, for the different fixed modulus of G_5, the phase angle which achieves the optimal harmonic compensation performance can be approximated as a constant value. Similarly, the optimal phase angles for 7th and 11th harmonics can be obtained as 53 degree and 121 degree.

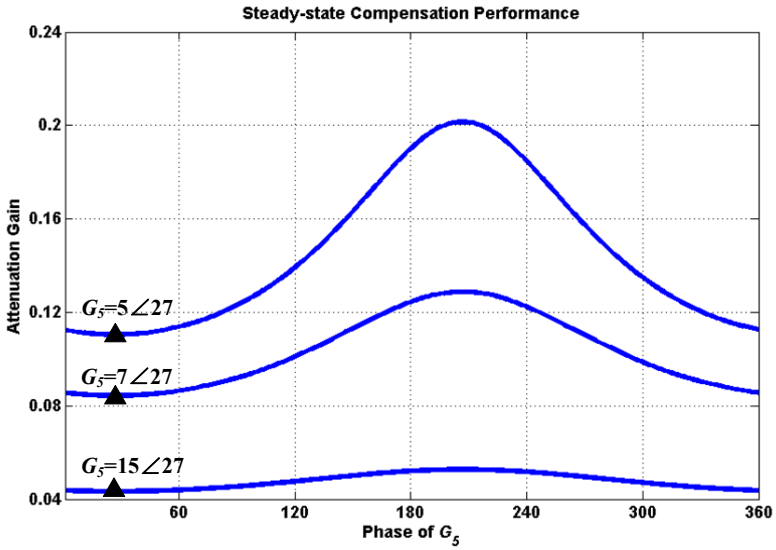

Fig. 3.10 Steady-state compensation performance for 5th harmonic when $|G_5|$ = 5, 7 and 15 under different phase angles (attenuation=$|I_{grid\_h}/I_{load\_h}|$)

Table 3.6 Harmonic compensation performance when the modulus of G is set as its maximum value with the optimal phase angle

	5th	7th	11th
Maximum $\|G\|$	55 (G_5=55∠27)	4 (G_7=4∠53)	1 (G_{11}=1∠121)
Attenuation ($\|I_{grid\_h}/I_{load\_h}\|$)	0.013	0.108	0.186

When the modulus of G is fixed, the complex number G whose phase angle is set as its optimal phase angle can provide a better harmonic compensation performance than real number G. But when the modulus of G is variable and the system stability is taken into account, the effectiveness of the complex G also needs to be investigated. Table 3.6 shows harmonic compensation performance when the modulus of G is set as its maximum value that makes the system stable and its phase angle is set as the corresponding optimal phase angle. Compared with Table 3.4, it can be seen that the harmonic compensation performance in Table 3.6 is worse than the one using real number G due to its poor system stability. Therefore, the virtual impedance using the specific complex number G that provides optimal compensation performance under fixed G modulus is also not suitable for the proposed method at relatively low switching frequency.

3.3 Summary

In this chapter, the system stability is investigated at first. The system stability is discussed when the modulus of harmonic compensation feedback gain G is set as a constant with different phase angles. And the modulus ranges of G that make the system stable under different angles are provided. Through the analysis, one can reach the conclusion that when the amplitude of G is fixed, setting G as a real number (the phase angle of G is 0 degree or 180 degree) can achieve the best system stability. And which is the most stable phase angle among 0 degree and 180 degree can be determined by checking if the harmonic equivalent impedance contains negative resistance or if G and $[Z_C / (Z_{L1}+Z_C)]$ are the same sign.

Then the virtual impedance design is discussed. Three design schemes are analyzed respectively. One is the virtual impedance using real number G. As mentioned previously, it is easy to implement and can provide satisfactory harmonic compensation performance and good system stability. The other two design schemes are virtual resistance using a proper complex number G, and virtual impedance using the complex number G whose phase angle is set as the angle that provides optimal harmonic compensation performance when the modulus of G is fixed. By comparing to the harmonic compensation performance of these two schemes, the harmonic compensation performance using real number G is much better because the good system stability allows the modulus of G to be set as a relatively large value. Although the virtual resistance and virtual impedance using a complex number G may have an effective compensation performance at high switching frequency, they are not flexible for the proposed method at low switching frequency.

Chapter 4

Simulation and Experimental Results

In order to verify the proposed harmonic compensation approach using DG interfacing converter with low switching frequency, both simulation and experiments are conducted and the simulation and experimental results are presented in this chapter. To facilitate the comparison of simulation and experiments results, the same system parameters are used for both simulation and experiments. The DG converter switching frequency adopted is 2 kHz.

4.1 Simulation Results

The proposed harmonic compensation method is firstly confirmed through Matlab/Simulink simulations. The configuration of single DG-grid system is the same as Fig. 2.1 and its parameters are listed in Table 4.1. A three-phase diode rectifier which is connected with parallel-connected capacitor and resistor at the dc side is used as the nonlinear load at PCC.

Table 4.1 Parameters of the single DG-grid system

Grid	L_g=5 mH, V_{grid}=52 V (60Hz, 3 phase)
Load (6-pulse diode rectifier)	L_{ac}=2.5 mH, C_{dc}=1000 uF, R_{dc}=8 ohm
LCL filter	L_1=2.5 mH, L_2=2.5 mH, C=40 uF, R_d=1 ohm
DG	V_{dc}=150 V
Switching Frequency	2 kHz

4.1.1 Harmonic compensation performance using a real number *G*

At first, the proposed harmonic compensation method is tested in the simulation with the 5^{th}, 7^{th} and 11^{th} harmonics compensated by real number *G*. Fig. 4.1 shows the performance of the DG without harmonic compensation. It can be seen that the nonlinear load current is provided by both the DG and the grid, and the PCC voltage is distorted due to the harmonic voltage drop on the grid impedance.

The performance of the DG with the proposed harmonic compensation method is shown in Fig. 4.2, in which the harmonic feedback gains are set as G_5=20, G_7=10 and G_{11}=-8. Although the maximum modulus value of the harmonic compensation gains that make the system stable are $|G_5|$=68, $|G_7|$=31 and $|G_{11}|$=17 as shown in Table 3.4, a too large harmonic compensation signal will cause the interaction among the 5^{th}, 7^{th} and 11^{th} harmonics compensation. In addition, based on Fig. 2.10 to Fig. 2.12 in Chapter 2, when the feedback gain is large enough, the effect of harmonic compensation changes little with the compensation gain increases. Therefore, the practical real number compensation feedback gain *G* is selected carefully in simulation and experiment (G_5=20, G_7=10 and G_{11}=-8), which could provide effective enough harmonic compensation. As can be seen in Fig. 4.2, the PCC voltage and grid current are improved significantly since the DG unit absorbs most of the nonlinear load currents by acting as small impedance at harmonic frequencies.

According to the harmonic analyses in Fig. 4.3 and Fig. 4.4, the THD of the PCC voltage is improved from 12.06% without harmonic compensation to 4.57% when the proposed harmonic control is applied. As expected, the proposed harmonic compensation method works well at a relatively low switching frequency (2 kHz).

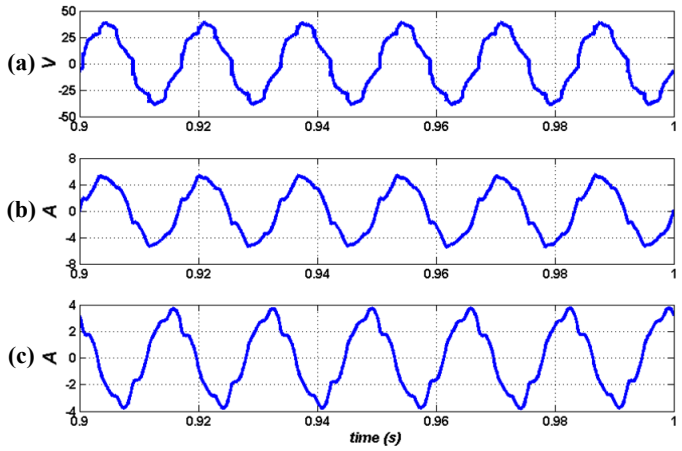

Fig. 4.1 Performance of DG without harmonic compensation. (a) PCC voltage. (b) DG current. (c) Grid current.

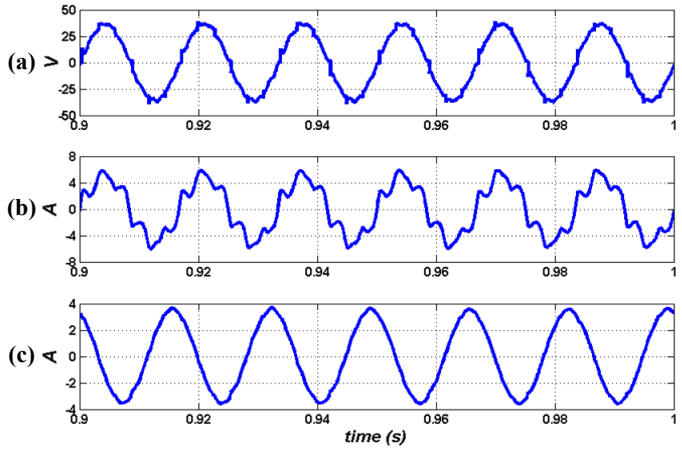

Fig. 4.2 Performance of DG with the proposed harmonic compensation method. (a) PCC voltage. (b) DG current. (c) Grid current. (G_5=20, G_7=10 and G_{11}=-8)

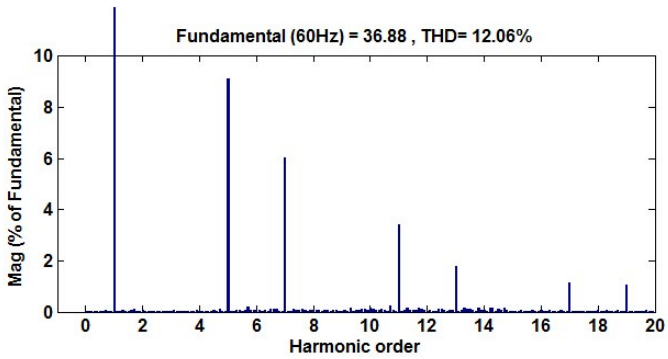

Fig. 4.3 Harmonic analysis of the PCC voltage without harmonic compensation

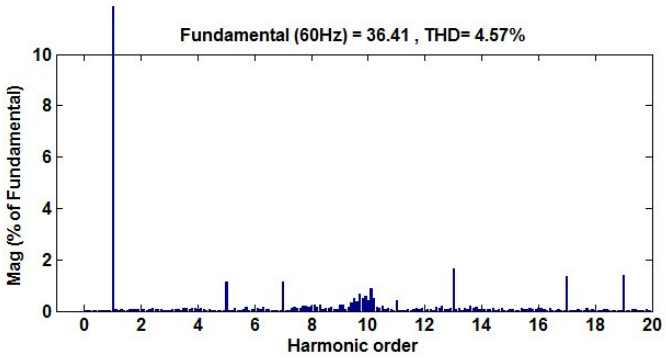

Fig. 4.4 Harmonic analysis of the PCC voltage with harmonic compensation (G_5=20, G_7=10 and G_{11}=-8)

4.1.2 Harmonic compensation performance using a virtual resistance

The proposed harmonic compensation method using a virtual resistance is also tested in the simulation. As shown in Table 3.5 in Chapter 3, the minimum virtual resistances (R_5=2.3 Ω, R_7=4.4 Ω and R_{11}=0.5 Ω) that make the system stable, and corresponding harmonic feedback gains (G_5=2.27∠101.17, G_7=1.27∠143.56 and G_{11}=13.56∠177.18) are obtained. Fig. 4.5 shows the performance of DG when it is controlled to be the minimum virtual resistance at harmonic frequencies. It can be observed that, compared with the waveform performance without harmonic compensation, the waveforms of the PCC voltage and the grid current in Fig. 4.5 only improve slightly. The THD of the PCC voltage is improved from 12.06% without harmonic compensation to 8.45% as shown in Fig. 4.6.

The simulation results agree with the previous analysis. Due to the system stability limit, the 5th and 7th harmonics are only mitigated slightly. However, the 11th harmonic is improved significantly from 3.39% to 0.26% since the phase angle of G_{11} when using virtual resistance is very close to its most stable angle (180 degree).

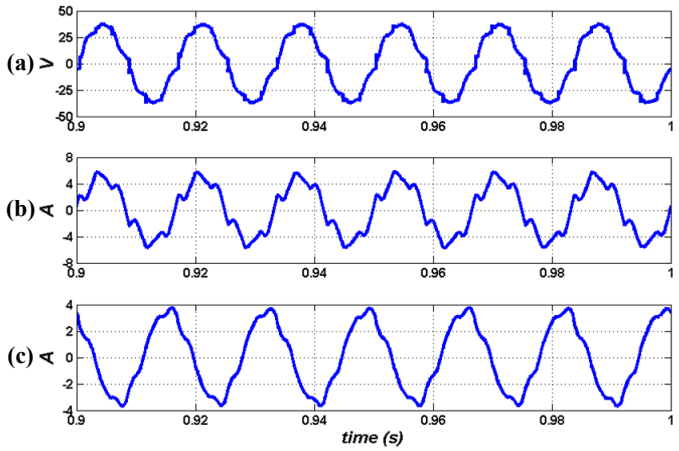

Fig. 4.5 Performance of DG with the harmonic compensation using virtual resistance. (a) PCC voltage. (b) DG current. (c) Grid current. (G_5=2.27∠101.17, G_7=1.27∠143.56 and G_{11}=13.56∠177.18)

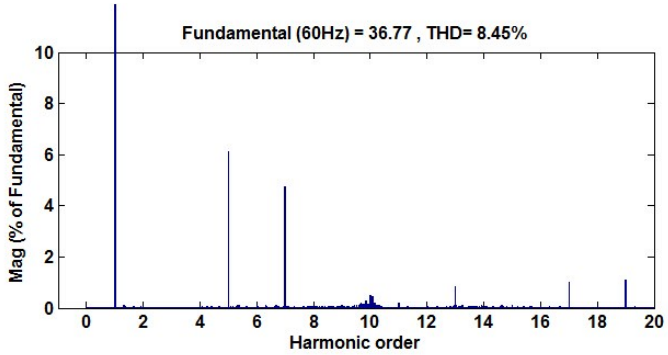

Fig. 4.6 Harmonic analysis of the PCC voltage with harmonic compensation using virtual resistance (G_5=2.27∠101.17, G_7=1.27∠143.56 and G_{11}=13.56∠177.18)

4.2 Experimental Results

To experimentally validate the proposed harmonic compensation method, experiments have been carried out on a grid connected three-phase DG in the lab as shown in Fig. 4.7. The experiment parameters are the same with the simulation parameters as listed in Table 4.1. A dSPACE (DS1103) control system is used to control the DG-grid interfacing converter. And the grid voltage is provided by a three-phase programmable power supply. The nonlinear load is also a three-phase diode rectifier with parallel-connected capacitor and resistor at dc side.

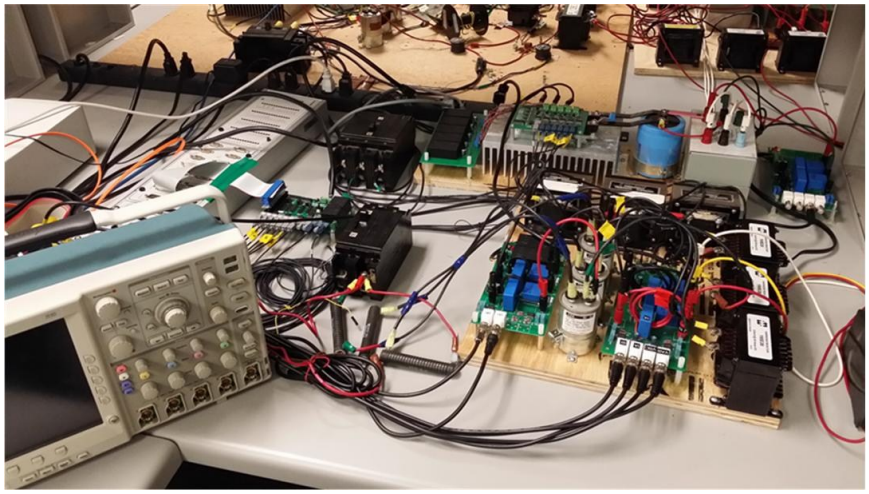

Fig. 4.7 Experimental system with a grid connected three-phase DG

4.2.1 Harmonic compensation performance using a real number *G*

The performance of DG without harmonic compensation is shown in Fig. 4.8, and the harmonic analysis of the PCC voltage is shown in Fig. 4.9. As shown, without harmonic compensation, the THD of the PCC voltage is 11.03%, and the 5^{th}, 7^{th} and 11^{th} harmonics are 7.92%, 5.69% and 4.30% respectively.

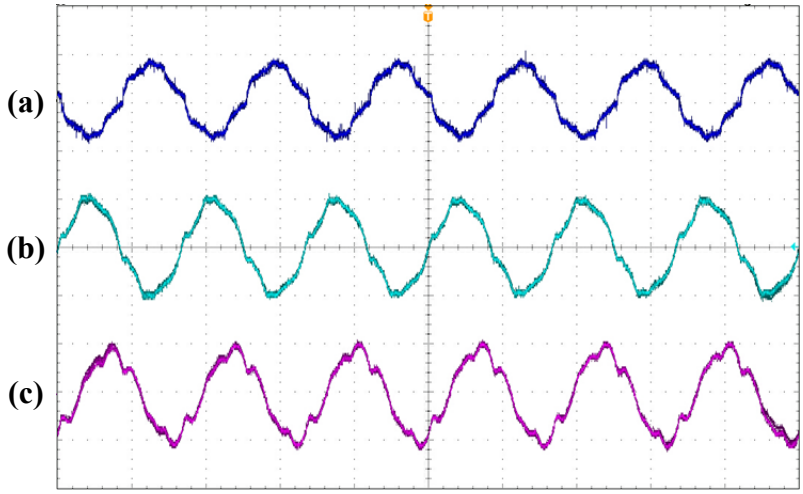

Fig. 4.8 Performance of DG without harmonic compensation. (a) PCC voltage (50 V/div). (b) DG current (5 A/div). (c) Grid current (2.5 A/div).

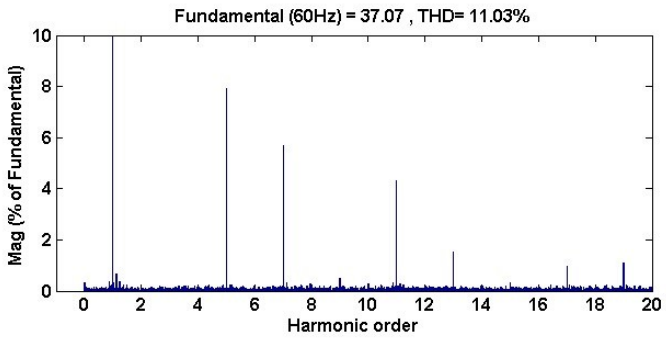

Fig. 4.9 Harmonic analysis of the PCC voltage without harmonic compensation (THD=11.03%, h_5=7.92%, h_7=5.69% and h_{11}=4.30%)

When the proposed harmonic compensation is implemented to compensate 5th harmonic (with a real number G_5=20), both the PCC voltage and the grid current are improved effectively at 5th harmonic frequency as shown in Fig. 4.10 and Fig. 4.11. With the 5th harmonic compensation, the THD of the PCC voltage is decreased from 11.03% to 8.49% and the 5th harmonic h_5 is decreased from 7.92% to 1.35%. It is worthwhile to note that the 7th harmonic increases from 5.69% to 6.83% when compensating the 5th harmonic. A high value of real number G_5 may have negative impact on compensating the other order harmonics. Therefore, a practical limitation of G should be selected carefully.

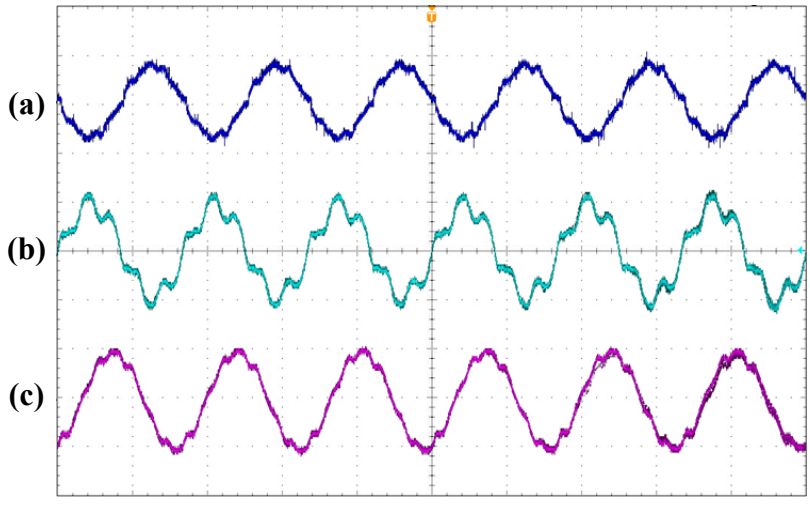

Fig. 4.10 Performance of DG with 5th harmonic compensation. (a) PCC voltage (50 V/div). (b) DG current (5 A/div). (c) Grid current (2.5 A/div). (G_5=20)

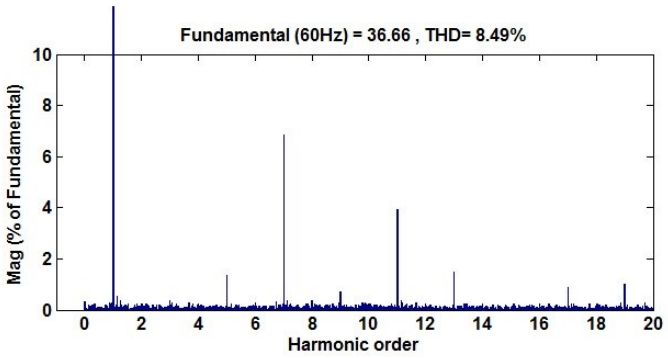

Fig. 4.11 Harmonic analysis of the PCC voltage with 5th harmonic compensation (THD=8.49%, h_5=1.35%, h_7=6.83% and h_{11}=3.93%)

Similarly, the performance of DG with 7th harmonic compensation and the harmonic analysis of the PCC voltage are shown in Fig. 4.12 and Fig. 4.13, in which the 7th harmonic is improved form 5.69% to 1.86%.

The performance of DG with 11th harmonic compensation and the harmonic analysis of the PCC voltage are shown in Fig. 4.14 and Fig. 4.15 where the 11th harmonic is improved form 4.30% without compensation to 0.40%.

Then the performance of the DG when the proposed harmonic compensation method is implemented to compensate 5th, 7th and 11th harmonics is shown in Fig. 4.16, in which the harmonic feedback gains are set as G_5=20, G_7=10 and G_{11}=-8. It can be seen that most harmonic currents of the nonlinear load are absorbed by the DG unit leaving an improved PCC voltage and grid current with lower THD. As shown in Fig. 4.17, the THD of the PCC voltage is reduced from 11.03% without compensation to 4.12% when the proposed method is applied. As a result, when the feedback gain G is set as a real number, the effectiveness of the proposed harmonic control method at a relatively low switching frequency is verified in the experiments.

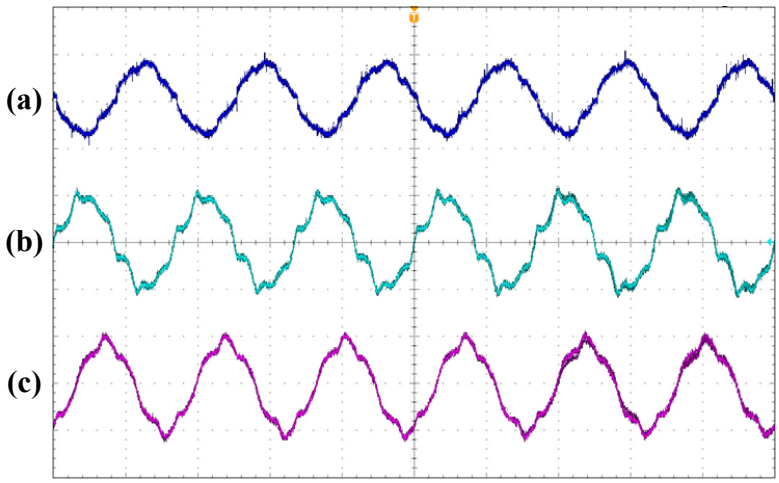

Fig. 4.12 Performance of DG with 7th harmonic compensation. (a) PCC voltage (50 V/div). (b) DG current (5 A/div). (c) Grid current (2.5 A/div). (G_7=10)

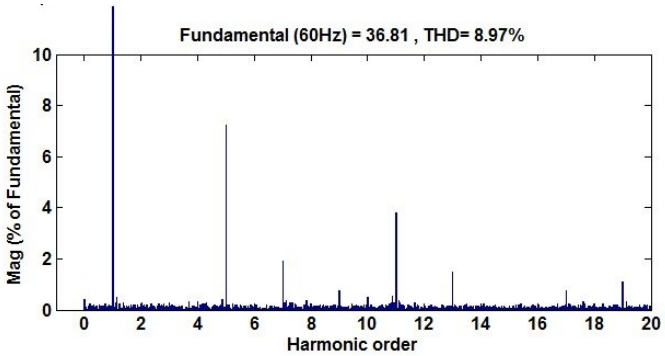

Fig. 4.13 Harmonic analysis of the PCC voltage with 7th harmonic compensation (THD=8.97%, h_5=7.22%, h_7=1.86% and h_{11}=3.78%)

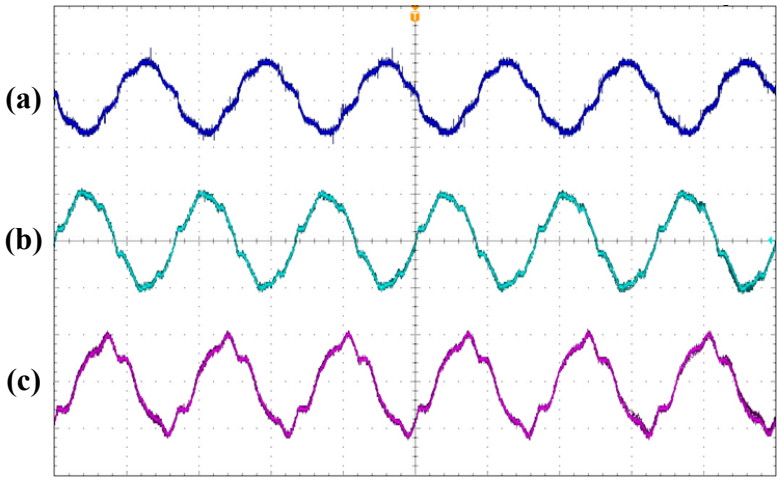

Fig. 4.14 Performance of DG with 11th harmonic compensation. (a) PCC voltage (50 V/div). (b) DG current (5 A/div). (c) Grid current (2.5 A/div). (G_{11}=-8)

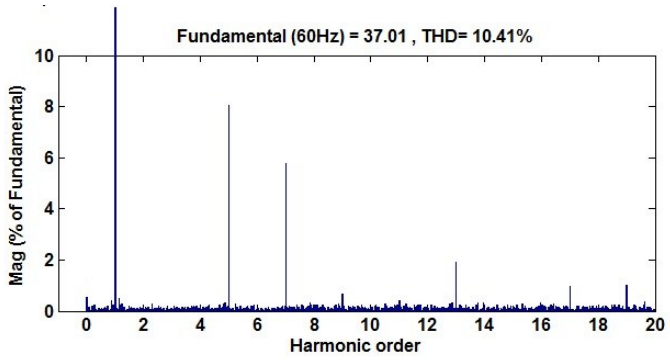

Fig. 4.15 Harmonic analysis of the PCC voltage with 11th harmonic compensation (THD=10.41%, h_5=8.03%, h_7=5.75% and h_{11}=0.40%)

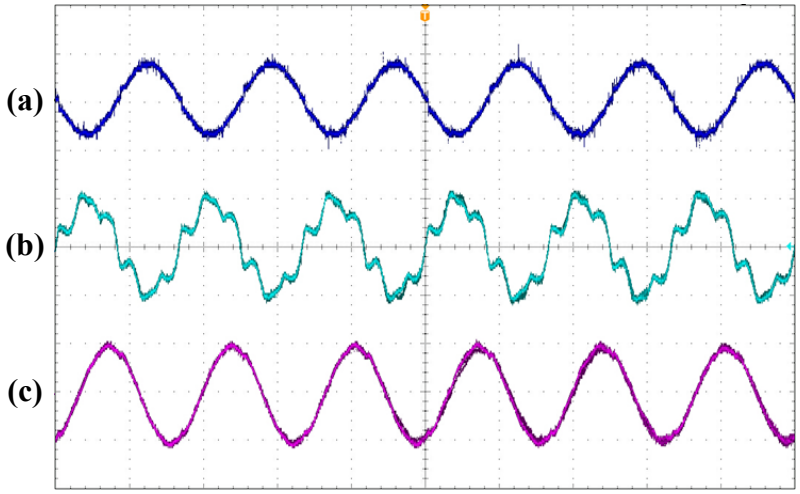

Fig. 4.16 Performance of DG with harmonic compensation. (a) PCC voltage (50 V/div). (b) DG current (5 A/div). (c) Grid current (2.5 A/div). (G_5=20, G_7=10 and G_{11}=-8)

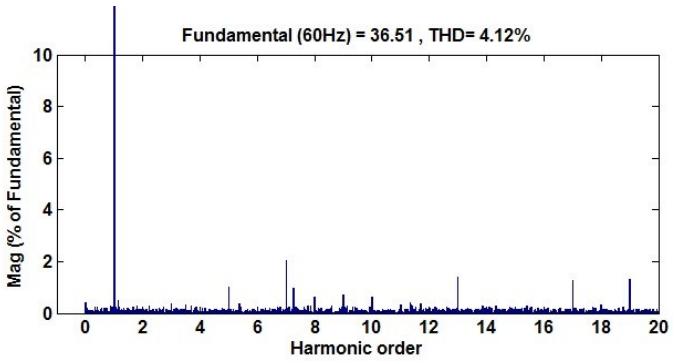

Fig. 4.17 Harmonic analysis of the PCC voltage with harmonic compensation (THD=4.12%, h_5=1.01%, h_7=2.02% and h_{11}=0.34%)

4.2.2 Harmonic compensation performance using a virtual resistance

In order to demonstrate the effectiveness of the proposed method when the DG unit equivalent impedance is controlled to be a resistance, the corresponding experimental results are also obtained. The performance of DG when the virtual resistances at harmonic frequencies are controlled properly to be their minimum values (R_5=2.3 Ω, R_7=4.4 Ω and R_{11}=0.5 Ω), and the harmonic analysis of the PCC voltage are shown in Fig. 4.18 and Fig. 4.19 respectively. The THD of the PCC voltage is reduced from11.03% to 6.90%. Compared with real number G, the harmonic compensation performance using virtual resistance are limited by poor system stability. Therefore, virtual resistance is not flexible for the proposed harmonic compensation method at relatively low switching frequency.

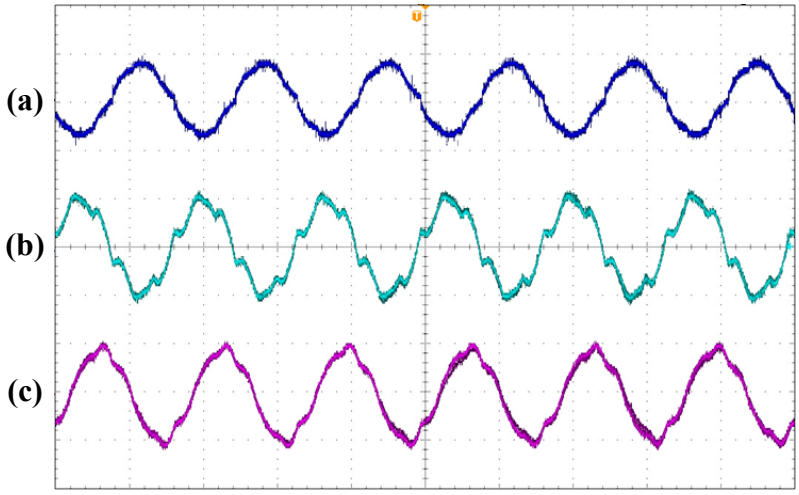

Fig. 4.18 Performance of DG with harmonic compensation using virtual resistance. (a) PCC voltage (50 V/div). (b) DG current (5 A/div). (c) Grid current (2.5 A/div). (G_5=2.27∠101.17, G_7=1.27∠143.56 and G_{11}=13.56∠177.18)

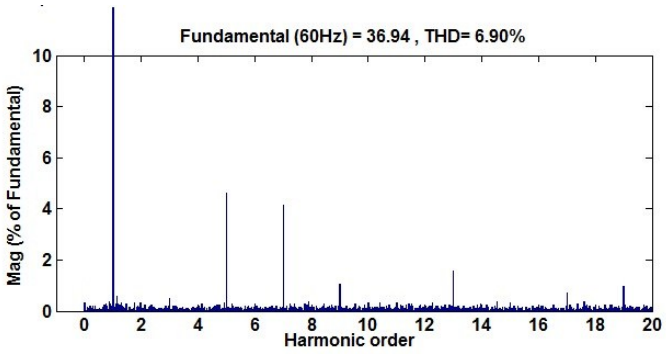

Fig. 4.19 Harmonic analysis of the PCC voltage with harmonic compensation using virtual resistance (G_5=2.27∠101.17, G_7=1.27∠143.56 and G_{11}=13.56∠177.18)

4.3 Summary

In this chapter, simulation and experiments are carried out to verify the proposed harmonics compensation method in Chapter 2, as well as the virtual impedance design in Chapter 3. The same system parameters and a low switching frequency of 2 kHz are adopted in both simulation and the experiments. The simulation and experimental results are in agreement and show that the proposed harmonic compensation method can effectively reduce the PCC voltage harmonics. Additionally it shows that the harmonics reduction performance is the best when a real number G is adopted as it has much better stability and therefore a larger gain can be selected. On the other hand, although a virtual resistor (with G being complex number) has advantages with R-APF characteristics, the minimum possible virtual resistor is limited due to the stability concern which compromised the harmonics mitigation performance.

Chapter 5

Conclusion and Future Work

5.1 Conclusion

This thesis proposes a new distribution system harmonic compensation approach using DG-grid interfacing converters. Although the conventional compensation method has an effective performance with high switching frequency, it does not work well at low switching frequency which is expected for high power DG interfacing converters to reduce switching losses. Through controlling the PWM reference signal directly for the harmonic component to avoid the multi-loop control path of the fundamental component, the proposed method can achieve the effective high order harmonics compensation.

In Chapter 2, the control scheme of proposed method is introduced in detail, and the simplified and full system models with the proposed harmonic control are established. Based on the full system model, the DG unit equivalent impedance can be controlled to be any specific virtual impedance as expected. And the simplified system model can be adopted to evaluate harmonic compensation performance for low order harmonics such as 5^{th} and 7^{th} harmonics since it is easy for calculation and the theoretical results of harmonic compensation performance of simplified model and full model are almost the same when the order of harmonic is low.

The virtual impedance design of the DG unit at harmonic frequencies is discussed in Chapter 3. According to the theoretical analysis of system stability and harmonic compensation performance, three virtual impedance design

schemes are investigated: virtual impedance using a real number harmonic feedback gain G, virtual resistance using a proper complex number G, and virtual impedance using the complex number harmonic feedback gain whose phase angle is set as the angle that provides optimal harmonic compensation performance when the modulus of G is fixed. The study reveals that the virtual impedance using a real number feedback gain is flexible and can provide the most effective harmonic compensation performance because of its good system stability. The simulation and experimental results are obtained and presented in Chapter 4. These results verify the effectiveness of the proposed harmonic compensation method in Chapter 2 and the virtual impedance design analysis in Chapter 3.

5.2 Future Work

To further develop the proposed idea of harmonics control with low switching frequency converter, the following considerations are recommended for future work.

Firstly, if controlled properly, the DG unit equivalent impedance can increase at harmonic frequencies to reject harmonics so that the DG unit has lower harmonics and better THD to meet today's grid connection requirements. This operation mode is called harmonic rejection mode. To realize a large virtual impedance at harmonic frequencies, the virtual impedance design and stability analysis of DG operating in the harmonic rejection mode would be an important topic for further study.

Secondly, the harmonic feedback gain G is set as a fixed value in the proposed method. However, the DG unit should be controlled with variable harmonic compensation levels when its available apparent power for harmonic compensation is changing (with the variation of DG real power output). Therefore an algorithm that can automatically adjust the compensation gain according to the desired harmonics compensation level should be developed.

In addition, when the proposed harmonic control is applied to a large number of interfacing converters in a multiple DG system, they may interact and compete with each other for harmonic compensation. A study of the possible interaction of multiple DGs in harmonics compensation operation can be carried out, and the most suitable virtual impedance for multiple DG situations can be designed.

Reference

[1] F. Katiraei and M. R. Iravani, "Power management strategies for a microgrid with multiple distributed generation units," *IEEE Trans. Power Syst.*, vol. 21, no. 4, pp. 1821–1831, Nov. 2006.

[2] W. EI-Khattam, Y. G. Hegazy, and M.M.A. Salama, "An integrated distributed generation optimization model for distribution system planning," *IEEE Trans. Power Syst.*, vol. 20, no.2, pp. 1158-1165, May. 2005.

[3] A. Keane and M. O'Malley, "Optimal allocation of embedded generation on distribution networks," *IEEE Trans. Power Syst.*, vol. 20, no.3, pp. 1640-1646, Aug. 2005.

[4] N. S. Rau and Y. H. Wan, "Optimum location of resources in distributed planning," *IEEE Trans. Power Syst.*, vol. 9, no. 4, pp. 2014–2020, Nov. 1994.

[5] J.M. Carrasco, L. G. Franquelo, and J. T. Bialasiewicz, "Power-electronic systems for the grid integration of renewable energy sources: A survey," *IEEE Trans. Ind. Electron.*, vol. 53, no. 4, pp. 1002–1016, Aug. 2006.

[6] F. Blaabjerg, Z. Chen, and S. B. Kjaer, "Power electronics as efficient interface in dispersed power generation systems," *IEEE Trans. Power Electron.*, vol. 19, no. 5, pp. 1184–1194, Sep. 2004.

[7] M. Triggianese, F. Liccardo, and P.Marino, "Ancillary services performed by distributed generation in grid integration," in *Proc. IEEE Int. Conf. Clean Elect. Power*, 2007, pp. 164–170.

[8] P. T. Cheng, C. Chen, T. L. Lee, and S. Y. Kuo, "A cooperative imbalance compensation method for distributed-generation interface converters," *IEEE Trans. Ind. Appl.*, vol. 45, no. 2, pp. 805–815, Mar./Apr. 2009.

[9] M. Savaghebi, A. Jalilian, J. C. Vasquez, and J. M. Guerrero, "Autonomous voltage unbalance compensation in an island droop-controlled microgrid," *IEEE Trans. Ind. Electron*., vol. 60, no. 4, pp. 1390-1402, Apr. 2013.

[10] Y. Li, D. M. Vilathgamuwa, and P. C. Loh, "Microgrid power quality enhancement using a three-phase four-wire grid-interfacing compensator," *IEEE Trans. Ind. Appl.*, vol. 41, no. 6, pp. 1707–1719,Nov./Dec. 2005.

[11] J. He, Y. W. Li, and M. S. Munir, "A flexible harmonic control approach through voltage controlled DG-grid interfacing converters," *IEEE Trans. Ind. Electron.*, vol. 59, no. 1, pp. 444-455, Jan. 2012.

[12] J. He, S. Munir, and Y. W. Li, "Opportunities for power quality improvement through DG–grid interfacing converters," in *Conf. Rec. IEEE IPEC*, 2010, pp. 1657–1664.

[13] T. Takeshita and N. Matsui, "Current waveform control of PWM converter

system for harmonic suppression on distribution system," *IEEE Trans. Ind. Electron.*, vol. 50, no. 6, pp. 1134-1139, Dec. 2003.

[14] M. Cirrincione, M. Pucci, and G. Vitale, "A single-phase DG generation unit with shunt active power filter capability by adaptive neural filtering," *IEEE Trans. Ind. Electron.*, vol. 55, no. 5, pp. 2093–2110, May 2008.

[15] C. J. Gajanayake, D. M. Vilathgamuwa, P. C. Loh, R. Teodorescu, and F. Blaabjerg, "Z-source-inverter-based flexible distributed generation system solution for grid power quality improvement," *IEEE Trans. Energy Convers.*, vol. 24, no. 3, pp. 695–704, Sep. 2009.

[16] N. Pogaku and T. C. Green, "Harmonic mitigation throughout a distribution system: A distributed-generator-based solution," *Proc. Inst. Elect. Eng.-Gener. Transmiss. Distrib.*, vol. 153, no. 3, pp. 350–358, May 2006.

[17] M. I. Marei, T. K. Abdel-Galil, E. F. El-Saadany, and M. M. A. Salama, "Hilbert transform based control algorithm of the DG interface for voltage flicker mitigation," *IEEE Trans. Power Del.*, vol. 20, no. 2, pp. 1129–1133, Apr. 2005.

[18] G. Joos, B. T. Ooi, D. cGillis, F. D. Galiana, and R. Marceau, "The potential of distributed generation to provide ancillary services," in *Proc. IEEE Power Eng. Soc. Summer Meeting 2000*, Jul. 2000, vol. 3, pp. 1762–1767.

[19] W. M. Grady, M. J. Samotyj, and A. H. Noyola, "Survey of active line conditioning methodologies," *IEEE Trans. Power Del.*, vol. 5, no. 3, pp. 1536–1542, Jul. 1990.

[20] H. Akagi, "New trends in active filters for power conditioning," *IEEE Trans. Ind. Appl.*, vol. 32, no. 2, pp. 1312–1332, Nov./Dec. 1996.

[21] H. Akagi, H. Fujita, and K. Wada, "A shunt active filter based on voltage detection for harmonic termination of a radial power distribution line," *IEEE Trans. Ind. Appl.*, vol. 35, no. 3, pp. 638–645, May/Jun. 1999.

[22] M. Cirrincione, M. Pucci, and G. Vitale, "A single-phase DG generation unit with shunt active power filter capability by adaptive neural filtering," *IEEE Trans. Ind. Electron.*, vol. 55, no. 5, pp. 2093–2110, May 2008.

[23] M. Routimo, M. Salo, and H. Tussa, "Comparison of voltage-source and current-source shunt active power filter," *IEEE Trans. Power Electron.*, vol. 22, no. 2, pp. 636-643, Mar. 2007.

[24] F. Z. Peng, H. Akagi, and A. Nabae, "Compensation characteristics of the combined system of shunt passive and series active filters," *IEEE Trans. Ind. Appl.*, vol. 29, no. 1, pp. 144-152, Jan/Feb. 1993.

[25] M. Rastogi, N. Mohan, and A. Edris, "Hybrid-active filtering of harmonic currents in power systems", *IEEE Trans. Power Delivery,* vol. 10, pp. 1994-2000, Oct. 1995.

[26] T.C. Green and J.H. Marks, "Control techniques for active power filters,"

Proc. Inst. Electr. Eng. Electr. Power Appl., vol. 152, no. 2, pp.369-381, Mar. 2005.

[27] H. Akagi , Y. Kanazawa, and A. Nabae, "Instantaneous reactive power compensators comprising switching devices without energy storage components," *IEEE Trans. Ind. Appl.*, vol. IA-20, no. 3, pp. 625-630, May/Jun. 1984.

[28] Y. W. Li, "Control and resonance damping of voltage source and current source converters with LC filters," *IEEE Trans. Ind. Electron.*, vol. 56, no. 5, pp. 1511–1521, May 2009.

[29] D. N. Zmood and D. G. Holmes, "Stationary frame current regulation of PWM inverters with zero steady-state error," *IEEE Trans. Power Electron.*, vol. 18, no. 3, pp. 814–822, May 2003.

[30] E. Jacobsen and R. Lyons, "The sliding DFT," *IEEE Signal Process. Mag.*, vol. 20, no. 2, pp. 74–80, Mar. 2003.

[31] N. Pogaku and T. C. Green, "Harmonic mitigation throughout a distribution system: A distributed-generator-based solution," *Proc. Inst. Elect. Eng.—Gener. Transm. Distrib.*, vol. 153, no. 3, pp. 350–358, May 11, 2006.

[32] T.-L. Lee, J.-C. Li, and P.-T. Cheng, "Discrete frequency tuning active filter for power system harmonics," *IEEE Trans. Power Electron.*, vol. 24, no. 5, pp. 1209–1217, May 2009.

[33] T. L. Lee and P. T. Cheng, "Design of a new cooperative harmonic filtering strategy for distributed generation interface converters in an islanding network," *IEEE Trans. Power Electron.*, vol. 22, no. 5, pp. 1919-1927, Sep. 2007.

[34] M. Liserre, F. Blaabjerg, and S. Hansen, "Design and control of an LCL-filter based three-phase active rectifier," *IEEE Trans. Ind. Appl.*, vol. 41, no. 5, pp. 1281–1291, Sep./Oct. 2005.

[35] Y. Tang, P. C. Loh, P. Wang, F. H. Choo, F. Gao, and F. Blaabjerg, "Generalized design of high performance shunt active power filter with output LCL filter," *IEEE Trans. Ind. Electron.*, vol. 59, no. 3, pp. 1443–1452, Mar. 2012.

[36] I. J. Gabe, V. F. Montagner, and H. Pinheiro, "Design and implementation of a robust current controller for VSI connected to the grid through an LCL filter," *IEEE Trans. Power Electron.*, vol. 24, no. 6, pp. 1444–1452, Jun. 2009.

[37] D. Pan, X. Ruan, C. Bao, W. Li, and X. Wang, "Capacitor-current-feedback active damping with reduced computation delay for improving robustness of LCL-type grid-connected inverter," *IEEE Trans. Power Electron.*, vol. 29, no. 7, pp. 3414–3427, Jul. 2014.